Student thesis series INES nr 556

Testing the potential to evaluate vegetation optical depth with ecosystem water dynamics in a temperate forest

Ainahu Abdul Hamid

2021
Department of
Physical Geography and Ecosystem Science
Lund University
Sölvegatan 12
S-223 62 Lund
Sweden

Ainahu Abdul Hamid (2021).

Testing the potential to evaluate vegetation optical depth with ecosystem water dynamics in a temperate forest

Testa potentialen för att utvärdera vegetationsoptiskt djup med ekosystemets vattendynamik i en tempererad skog

Master's degree thesis, 30 credits in *Subject of degree*
Department of Physical Geography and Ecosystem Science, Lund University

Level: Master of Science (MSc)

Course duration: *January* 2021 until *June* 2021

Testing the potential to evaluate vegetation optical depth with ecosystem water dynamics in a temperate forest

---

Ainahu Abdul Hamid

Master thesis, 30 credits, in *Physical Geography and Ecosystem Science*

Supervisor name
Thomas Pugh, Lund University

Exam Committee:
Lena Ström, Lund University
Aradhana Roberts, Lund University

Abstract

Warming trends have been associated with drought which induces and heightens agents and factors that cause tree mortality. Remotely sensed observations are increasingly being used in vegetation studies and are obtained from Earth observation satellites. Vegetation optical depth (VOD) is one such product and is obtained from the microwave domain, both passive and active. It measures the degree of attenuation of microwave waves within the canopy and relates to its above-ground biomass and relative water content. Despite the advancement in terrestrial and ecosystem modeling, models are unable to accurately represent or forecast mortality events. However, with more tree mortality being anticipated with climate change, model development is key to better understanding and forecasting. Thus, the dynamic vegetation model, LPJ-GUESS has been updated with a plant hydraulics formulation to simulate leaf water potential, to improve simulations of drought-induced tree mortality. This research seeks to explain variations in the VOD of two deciduous broadleaf forests in North America, as a function of temperature, precipitation, vapor pressure deficit, and LPJ-GUESS simulation of evapotranspiration and leaf water potential. Correlation results show that temperature has a strong influence on VOD and mostly combines with precipitation effects. Model simulation of evapotranspiration and leaf water potential failed to provide a better correlation to VOD than climatic variables. This research reinforces the importance of temperature and precipitation in monitoring tree mortality while highlighting the complexity of the processes that lead to tree mortality. Thus, the need for more information on factors such as tree size, basal area, genotype, slope, terrain, amongst others and a deep understanding of how they interact with each other is key in dissecting VOD signals, understanding mortality, and parameterizing ecosystem models for better model simulation of mortality scenarios.

Acronyms

VOD	Vegetation optical depth
RWC	Relative water content
PFTs	Plant functional types
LWP	Leaf water potential
VPD	Vapor pressure deficit
VODCA	Vegetation Optical Depth Climate Archive
SSM/I	Special Sensor Microwave/Imager
TMI	Tropical Rainfall Measuring Mission
AMSR-E	Radiometer – Earth Observing System
CDF	Cumulative distribution function
NDVI	Normalized difference vegetation index
EVI	Enhanced vegetation index
LAI	Leaf area index
SOS	Start of Season
GPP	Gross primary production
GLDAS	Global Land Data Assimilation System
ET	Evapotranspiration

Table of Contents

Testing the potential to evaluate vegetation optical depth with ecosystem water dynamics in a temperate forest

Keywords: Vegetation optical depth; Temperate Forest; Climate; LPJ-GUESS; Evapotranspiration; Leaf water potential; Isohydricity; Hydraulic failure; Carbon starvation

1 Introduction

Extensive tree mortality events have been observed and continuously linked to severe drought events (Breshears and Allen 2002; McDowell et al. 2008), which are anticipated to become more frequent with climate change (Park Williams et al. 2013; Cook et al. 2015). Droughts have the propensity to cause wide-reaching shifts in plant function, structure, and community dynamics (Wolf et al. 2013) as well as increased risk of fires due to increased fuel loads (Bigler and Veblen 2011). These encapsulate the need for accurate monitoring and forecasting of tree mortality.

Remote sensing is becoming a convenient tool for monitoring mortality as it clears some key disadvantages associated with traditional forest inventory techniques (i.e. labor-intensive, limited in both time and space) (Rao et al. 2019). Notwithstanding the benefits of remote sensing techniques, it still has a long way to go. With more tree mortality being anticipated with climate change, there is the need to improve the ability of vegetation models to accurately capture tree mortality, which they are currently not so good at. Since mortality is linked to water dynamics, including representations of plant hydraulics in dynamic vegetation models should enable the representation of hydraulic failure, which is increasingly recognized as an important basis for tree death (Rowland et al. 2015; Schuldt et al. 2020; Arend et al. 2021), however, those hydraulic representations are difficult to evaluate over the large scale.
Emitted or reflected microwave radiation from the Earth's surface is attenuated by vegetation. The degree of attenuation can be derived from passive and active microwave satellite observations and is commonly referred to as vegetation optical depth (VOD) (Vreugdenhil et al. 2016). VOD is used in tree mortality studies as it relates to aboveground dry biomass (Liu et al. 2015) and its relative water content (Momen et al. 2017). VOD is potentially very useful because it gives an indication of plant water status and has been linked to leaf water potential (Konings and Gentine 2017). Thus, if we could evaluate VOD with the water dynamics of vegetation models it would be monumental in tree mortality studies. As then we would have a large-scale model to evaluate large-scale measurements with and vice versa.

To this end, the VOD of two deciduous broadleaf-dominated forests in North America will be examined. North America was selected because it is a temperate climatic zone where VOD observations are more reliable (Konings and Gentine 2017). Another motivation of the study location is the presence of large forest areas that are enough to cover the 25 km x 25 km VOD pixel and thus making signal interpretation simpler. In testing evaluator indices for VOD, various authors have used different indicators. For

instance, Rao et al (2019) used a variety of vegetation, topographic and climatic variables to try to explain variations in VOD, while Konings and Gentine (2017) utilized relative water content (RWC). In this research, climatic variables and chiefly evapotranspiration and leaf water potential simulated by the experimental version of LPJ-GUESS will be used as evaluator index to explain temporal variations in VOD.

LPJ-GUESS is a dynamic vegetation model that simulates the structure and dynamics of terrestrial ecosystems at landscape, regional and global scales. The framework is made up of several modules (or sub-models), each containing formulations of a relatively well-defined, related subset of ecosystem processes with a distinct spatial and/or temporal signature (Smith et al. 2014). The dynamics of vegetation growth in the model are a consequence of growth and competitiveness for light, soil resources, and space. This competition is simulated in each grid cell among the woody plant individuals and the weedy or herbaceous understory. The totality of the simulated patches is considered to constitute the distribution of vegetation within a landscape. Woody tree types are categorized within the model as plant functional types (PFTs – trees, and shrubs). Amongst the simulations done on a daily time step are stomatal conductance, photosynthesis, respiration, and phenology. Net primary production gathered at the end of each simulation is then apportioned to fine roots, leaves, and sapwood per stipulated allometric relations for each PFT. The current resource status, demography, and life-history traits of each PFT influence the population dynamics of establishment and mortality and are represented as stochastic processes (Hickler et al. 2004; Wramneby et al. 2008).

Leaf water potential (LWP) measures the plant water status (Deloire and Heyns 2011); thus, its dynamics have been considered in studies of vegetation water stress. LWP is being used to explain VOD variations as it reflects the plant hydraulic status and is firmly linked to stomatal closure and xylem embolism (Jarvis, 1976; Sperry and Tyree 1988 as cited in Momen et al. 2017) which influences drought-driven tree mortality rates and biomass declines (Konings and Gentine 2017). Just like LWP, evapotranspiration is being considered as it combines the demand and supply aspects of water dynamics.

Vapor pressure deficit is influenced by temperature and humidity and refers to the difference between the actual vapor pressure of air and the vapor pressure of saturated air at the same temperature. VPD is the driving force for evapotranspiration and the movement of water through the soil-plant-atmosphere continuum. Water that is lost by transpiration at the leaf surface is replaced by the movement of water through the plant under tension as it is “sucked up” through the xylem vessels. Hence, the water potential gradient and resistance to water movement govern the rate of water movement through the plant (Chapin III et al. 2011).

This research seeks to investigate the temporal variability of VOD of two deciduous broadleaf forests in North America and how it relates to climatic variables namely, temperature, precipitation, vapor pressure deficit, and the ecosystem processes of evapotranspiration and leaf water potential. It is hypothesized that
(i) temperature and vapor pressure deficit will have an inverse relationship with VOD because higher temperatures influence soil moisture and cause higher vapor pressure deficits which leads to stomatal closure, lower carbon assimilation, and pronounced hydraulic limitation affecting VOD negatively

(ii) precipitation, evapotranspiration, and leaf water potential will have a direct relationship with VOD. This is because precipitation makes available water that is essential for photosynthesis and in so doing positively impacting VOD while evapotranspiration and leaf water potential are also driven by the change in pressure and movement of water between the soil and leaves indicating plant hydraulic status and strategy. The aims of this research are captured in the following research questions:

1. To what extent can temporal variability in VOD over broadleaf forests be explained by meteorological variables?

2. Does a process-based simulation of evapotranspiration and leaf water potential provide a better explanation of VOD than raw meteorological variables?

3. Is the explanatory power affected by the hydraulic strategy of the simulated vegetation?

2 Background

2.1 Mechanisms of Tree Mortality

Although the occurrence and consequences of tree mortality have been observed on every continent, knowledge about the defining causes is still unexpectedly lacking (McDowell et al 2008). However, it is contended by most authors that climate warming and thus elevated temperatures will exacerbate tree mortality. To aid the better understanding and forecasting of tree mortality McDowell et al (2008) hypothesized three mechanisms of drought-driven mortality. The mechanisms are hydraulic failure, carbon starvation, and biotic agent demographics.

The hydraulic-failure hypothesis speculates that the plant xylem conduit and rhizosphere may be caused to cavitate (become air-filled) due to decreased soil water supply combined with excessive evaporative demand ceasing the flow of water and desiccating plant tissues. The hydraulic-failure hypothesis is more probable when drought conditions are intense enough such that plants may exhaust water before carbon reserves and thus is based on the precept that complete desiccation leads to cellular death. On the hydraulic failure hypothesis, Hoffmann et al. (2011) and Rowland et al. (2015) discovered that between species with high wood density (large trees) and those with relatively low wood density (smaller trees), the former was more vulnerable to hydraulic failure in severe drought conditions than the latter. Hence dense wood species manifested substantial embolism and leaf desiccation. Meanwhile, Brodribb et al. (2010) investigated the linkage between cavitation and plant death for conifer species with varying degrees of water stress tolerance. Results indicate a strong linear relationship between water potential inducing a fifty percent loss of stem conductivity and the fatal water potential.

On the other hand, the carbon starvation hypothesis postulates that stomatal closure to avert hydraulic failure causes photosynthetic uptake of carbon to decrease. This results in plant carbon starvation due to continued demand for carbohydrates for metabolism and may be aggravated by heightened respiratory demands associated with higher temperatures during drought. Carbon starvation is more likely to occur

when drought is not severe enough to cause hydraulic failure but prolonged enough to deplete carbon reserves. Yoshimura et al. (2016) found that under drought conditions, stored carbon indeed contributes to tree survival.

In terms of the biotic agent demographics hypothesis McDowell et al (2008) propose that drought propel changes in demographics of mortality agents, such as pathogens and insects that eventually drive tree mortality. Increased number of pathogens per year due to temperature changes and lengthening of the growing season are some of the probable demographic changes that could occur. However, it is important to note that biotic agents can amplify hydraulic failure and carbon starvation and in the same vein be amplified by hydraulic failure and carbon starvation. Therefore, the three mechanisms may work inclusively and exclusively (McDowell et al. 2008).

2.2 Introduction to VOD

Vegetation optical depth is a dimensionless quantity ranging from 0 to 3 (Rao et al. 2019) and is obtained from the Global long-term microwave Vegetation Optical Depth Climate Archive (VODCA) (Moesinger et al. 2019). Measurements of radiation emitted by the Earth's surface have been captured and provided by space-borne microwave radiometers since the late 1970s and VOD is derived from such measurements. Since VOD is unaffected by clouds or high solar zenith angles and has a high temporal resolution of observations, it can be used to observe short-term to long-term changes in vegetation (Moesinger et al. 2020). This is because it is an indicator associated with the density, biomass, and water content of vegetation.

The VODCA archive is made up of VOD retrievals from multiple sensors such as Special Sensor Microwave/Imager (SSM/I), the Microwave Imager onboard the Tropical Rainfall Measuring Mission (TMI), the Advanced Microwave Scanning Radiometer – Earth Observing System (AMSR-E), WindSat, and AMSR2 using the Land Parameter Retrieval Model. Cumulative distribution function (CDF) matching was then used to co-calibrate the retrievals applying AMSR-E as the scaling reference. The datasets were then assembled by taking the arithmetic mean of temporally overlapping measurements after a matching technique that scales outliers more efficiently was applied (Moesinger et al. 2020). From these, 0.25-degree grid spatially sampled VOD microwave observations in different spectral bands are produced by VODCA. The VOD products range from the Ku-band (19 GHz, 1987-2017) to the X-band (10.7 GHz, 1997-2018), and the C-band (6.9 GHz, 2002-2018). A merit of using VOD in monitoring vegetation is that it has a slower saturation which culminates into higher sensitivity to high biomass (Liu et al. 2015) and thus has been used in several ecosystem studies.

For instance, Rao et al. (2019) used VOD to estimate relative water content which was then utilized as an empirical indicator for tree mortality. Jones et al. (2011) also used VOD to monitor global land surface phenology by correlating VOD with vegetation indices such as normalized difference vegetation index (NDVI), enhanced vegetation index (EVI), and leaf area index (LAI). Moreover, Jones et al. (2012) estimated the Start of Season (SOS) patterns of North America as well as its ecoregional annual variability using VOD and comparing it to MODIS green-up dates. Momen et al. (2017) went further by testing the sensitivity of VOD to leaf water potential and assessing its

ability to be used in constraining plant hydraulic models based on a conceptual framework developed from the sensitivity test. Plants are either isohydric or anisohydric depending on the continuum of xylem and stomatal regulation strategies that each species may display. Isohydric prone species are species that are inclined to keep their leaf water potential fairly steady during water stress while anisohydric species are those that allow significant fall in leaf water potential and are more liable to recurrent xylem embolism. Hence to aid in mortality studies by partitioning species based on the above strategies, Konings and Gentine (2017) used VOD to develop a metric of ecosystem-scale degree of isohydricity.

2.3 Ecosystem Modelling

Climatically crucial fluxes of carbon, energy, and water are impacted by terrestrial vegetation structure which is governed by ecological demographic processes (Bonan, 2008 as cited in Fisher et al. 2018). With the imminent threat of climate change at hand, there is growing consensus in the predictions of climate models towards drying and prolonged dry seasons (Joetzjer et al. 2013) despite variations in the spatial and temporal patterns (Jupp et al. 2010). Nonetheless, the ability of current ecosystem models to accurately represent the impacts of drought on forest ecosystems is still vague (Powell et al. 2013).

In wanting to examine the performance of models in predicting carbon fluxes during drought in the Amazon, Powell et al. (2013) evaluated the carbon flux predictions of five terrestrial biosphere models and one hydrodynamic terrestrial ecosystem model against measurements of two large-scale drought experiments. Findings from this study suggest that while the six models were able to reasonably replicate ecosystem carbon fluxes in the control plots; they failed to replicate the reactions to the drought treatments, notably the reductions in above-ground biomass and its associated carbon fluxes.

Bastos et al. (2021) also researched the vulnerability of European ecosystems to the dry and hot summers of 2018 and 2019 by assessing the ability of seven land-surface models to simulate the impacts of these two events. They found that while the models were able to simulate well the impacts of the 2018 drought on gross primary production (GPP), they performed poorly in simulating that of the succeeding drought of 2019. The authors attributed this limitation to a missing link in land-surface models which is the absence of processes controlling legacy effects. These processes are insect outbreaks, carbon starvation, damage from embolism, and its resultant tree death.

These findings and many others have repeatedly prompted the need for better representation of vegetation demographics especially plant hydraulics in ecosystem models as a critical step towards accurately simulating the impacts of droughts. On this basis, Hickler et al. (2006) took on the task of incorporating plant hydraulic architecture into the Lund-Potsdam-Jena Dynamic Global Vegetation Model (LPJ-DGVM).
To implement a more sophisticated hydraulic regime, they upgraded the previous bucket water supply model (Gerten et al. 2004 as cited in Hickler et al. 2006) to a new formulation where water supply is governed by a pressure gradient between the soil and the leaves and the resistance of fine roots, leaves, and sapwood. This formulation is based on Darcy's law (Whitehead, 1998 as cited in Hickler et al. 2006) and thus

determines the movement of water from the soil, through the roots, the xylem, and to the leaves. This upgrade made it feasible to sort out mechanistically the effects of hydraulic variation among plant functional groups on water cycling, competition, and vegetation structure (Hickler et al. 2006). Since then, Papastefanou et al. (in prep.) have also implemented an updated representation of plant hydraulics based on Hickler et al. (2006) as well as incorporating a new representation of leaf water potential (Papastefanou et al. 2020) into the LPJ-GUESS model.

To parameterize the range of plant strategies to simulating leaf water potential, a total of 28 plant functional types were defined based on different combinations of 7 defining functional traits related to plant hydraulics (Liu et al., in prep.). The functional traits are Maximum xylem conductivity per unit sapwood area (*Kstem*), Leaf area to sapwood area ratio (*LS*), Xylem water potential at 50% loss of conductivity (*P50*), Leaf turgor loss point (*TLP*), Wood density (*WD*), Leaf mass per unit area (*LMA*) and Xylem water potential at 88% loss of conductivity (*P88*) (see table 1 below). Liu et al. summarized these strategies in a principal component analysis to place the 28 plant functional types on a continuum of conservative vs risk-taking approaches to xylem construction and isohydricity vs anisohydricity (see section 2.2) (see figure 1). Conservative here implies species that invest a lot of resources into building higher wood density and hydraulic resilience while risk-taking species are those that invest into leaves and promote carbon capture instead of fortifying water supply (Reich 2014). Thus, the plant traits which is the common axis of variation determines how a species might react in drought conditions.

Table 1. Functional traits considered in this study (adapted from Liu et al. in prep.).

Symbol	Name	Units	Reasoning
Kstem	Maximum xylem conductivity per unit sapwood area	Kstem, kg m^{-1} s^{-1} Mpa^{-1}	Indicates maximum water flow rate to the canopy. Combined with information on atmospheric water demand, this will be linked to the total canopy area and degree of risk acceptable to that canopy.
LS	Leaf area to sapwood area ratio	ratio	Describes interrelation of sapwood-specific leaf conductivity and Kstem. Indicator of acquisitiveness of strategy, maximizing investment in carbon capture (high LS) versus ensuring water supply (LS).
P50	Xylem water potential at 50% loss of conductivity	MPa	A direct indicator of ability to withstand very high-water potential gradients.
TLP	Leaf turgor loss point	MPa	Closely correlated to isohydricity in the study of Fu and Meinzer (2019).
WD	Wood density	g cm^{-3}	Higher wood density has been widely related to more conservative strategies associated with greater investment in defense and/or hydraulic resilience.
LMA	Leaf mass per unit area	g m^{-2}	Higher investment in leaf tissue has been related to higher defensive allocation to protect that investment. Higher LMA also helps dissipate energy from high radiation inputs, protecting against high temperature.
P88	Xylem water potential at 88% loss of conductivity	MPa	A direct indicator of ability to withstand very high-water potential gradients. Considered to be the threshold for death by hydraulic failure (Hammond et al. 2019)

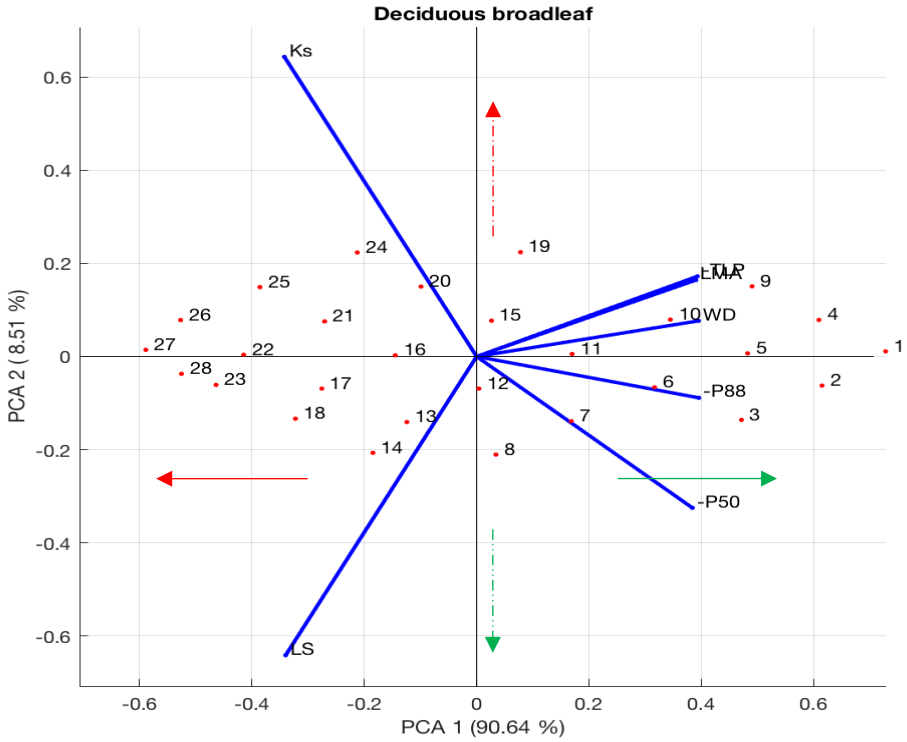

Figure 1: Principal component analysis displaying the positioning of the 28 plant functional types around the defining plant functional traits (*The red arrow for risk-taking: dashed red line for Anisohydric: Greenline for conservative: dashed green line for Isohydric strategy*) (adapted from Liu et al., in prep.).

3 Materials and Methods

3.1 Study Area

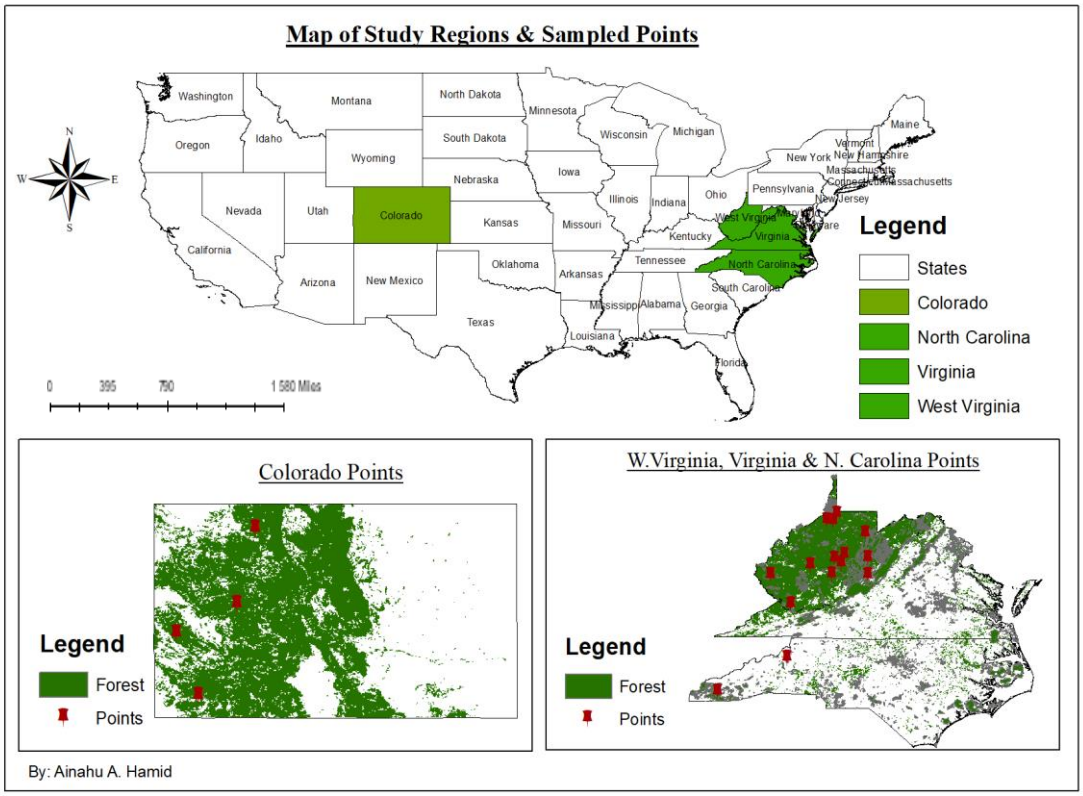

Figure 2: Map of the study region and sampled points in each study site (shapefiles obtained from U.S Geological Survey, 2021).

The target vegetation type for the study is broadleaf because conifers have not been parameterized yet in the experimental version of the LPJ-GUESS model. Therefore, deciduous broadleaf locations across the United States were carefully selected. One forest in the relatively low-lying West Virginia, Virginia, and North Carolina region (average elevation 650m) and the other in the higher elevation Western Colorado forest area (2245m). The state of Colorado is hereby referred to as the western study site and West Virginia, Virginia, and North Carolina as the eastern study site.

The mean annual precipitation for the eastern site is 1143 millimeters, annual average high and low temperature is 16 and 4 degrees Celsius, respectively (Runkle et al. 2017). Meanwhile, for the western site mean annual precipitation is 430 millimeters and the average annual temperature both high and low is 16 and 1 degree Celsius. Due to the elevation, mountainous topography, and climatic characteristics of the western side, it is cooler and drier (Frankson et al. 2017) as compared to the eastern side which is relatively warmer and wetter. While the eastern deciduous broadleaf forests contain birch, oak, aspen, black willow, and maple (Griffith and Widmann 2003), the western site is made up of narrow-leaf cottonwood, quaking aspen, plains cottonwood, gambel oak, and boxelder, amongst others (Colorado State Forest Service 2021).

In selecting the sampled points, one issue encountered is the coarseness of the VODCA VOD dataset which made it difficult to select grid cells purely covered by deciduous broadleaf trees. The grid cells were selected using the ESA CCI land cover (ESA CCI

2017). Since the eastern area has a continuous span of deciduous broadleaf trees obtaining the fifteen 25 km grid cells (15 was chosen as opposed to 1 to increase the confidence in VOD estimates) was fairly easy, but the difficulty was in obtaining pure grid cells as there are other types of vegetation within the forest area. Some of the other vegetation are natural vegetation such as shrubs, herbaceous plants, grasslands, as well as croplands. Grid cells with at least 80% deciduous broadleaf coverage were chosen. However, the western forest area only got a total of four grid cells because the deciduous broadleaf area was not big enough to obtain the fifteen grid cells. For the four grid cells, two contained some sparse shrubs, one containing about 15% needleleaf, and the other also had about 8% permanent snow and ice. It is important to state that the deciduous broadleaf forest of the western site is mostly surrounded by dense needleleaf.

3.2 Datasets

Table 2: Datasets utilized in the research

Name	Resolution	Period	Format
VOD	0.25°	1987 – 2017	NetCDF
Temperature	0.25°	1948 – 2010	-
Precipitation	0.25°	-	-
Vapor pressure deficit	0.25°	-	-
Plant Evapotranspiration	0.25°	1948 – 2010	-
Leaf water potential	0.25°	-	-

3.2.1 Vegetation Optical Depth

For this research, the Ku-band (19 GHz) was utilized to take advantage of the longer time span (1987-2017) as compared to the X-band and C-band. However, the key reason for choosing the Ku band is that it is closer in wavelength to the size of leaves and twigs which make up the canopy (as opposed to the trunk of trees)(Frappart et al. 2020). Moreover, during the CDF matching by Moesinger et al. (2020) they encountered a failure for the WindSat data. This failure affected all bands, but the Ku-band was the least affected with only 2 % of the grid points lost in comparison to the X-band with fails of 5% and C-band with 10% loss.
The data gaps present in both the eastern and western sites were mostly concentrated in the winter and spring months. The gaps were simply filled with the VOD value of the previously available reading because VOD changes slowly on daily timescales (Moesinger et al. 2020). Hence, short gaps can be filled with values of the days before or after (Konings et al. 2016).

3.2.2 Climate Variables

The climate variables that were used as explanatory indices for VOD are temperature, precipitation, and vapor pressure deficit. Temperature, precipitation, and vapor pressure deficit were selected because they serve as drivers of regional vegetation growth (Holdridge 1967) and tree mortality (McDowell et al. 2011). 25 km x 25 km climate dataset based on the coordinates of the chosen grid cells were retrieved from the Global Land Data Assimilation System (GLDAS) (Beaudoing et al. 2021) for consistency with the LPJ-GUESS model which also uses GLDAS climate data as input variables.

Temperature is in kelvin while precipitation is millimeters and vapor pressure deficit in kilopascals.

3.2.3 Evapotranspiration and Leaf Water Potential

Evapotranspiration (ET) and leaf water potential (LWP) were obtained as outputs of the ecosystem processes simulated by LPJ-GUESS. The resolution just like the climate variables is 25 km x 25 km. For evapotranspiration analysis, PFT 10 was used for both the eastern and western sites because temperature hardwoods have been identified to have high wood densities (Hoffmann et al. 2011; Nabais et al. 2018). To select the plant functional types for estimating leaf water potential, it is important to pay attention to the distinguishing traits and whether they coincide with that of the species under investigation. Thus, in estimating leaf water potential, a range of PFTs across the strategy spectrum were selected namely PFTs 12, 10, 15, 16, and 22.

3.3 Statistical Analysis

3.3.1 General Data Processing

All complete years of the VODCA dataset that overlapped with the period of the GLDAS climate data were taken, spanning 1988-2010. Thus, the statistical analysis was done on 23 years of data.

Daily values for the variables VOD, temperature, precipitation, vapor pressure deficit, evapotranspiration, and leaf water potential were averaged over all grid cells for each location. The averaged variables were filtered using a moving mean filter to remove the seasonal trends that might cause distortion in analysis and focus on the short-term variability. A window width of 3 and 14 was used to filter the monthly and daily variables, respectively (see Figures 3 & 4). The choice of window width was entirely influenced by the number of data points in the monthly (23 points) and daily (2116 – 2507 points) time series. Figure 3 and 4 shows an example (using the western site) of how the monthly and daily moving mean filter was applied. From this, the monthly, and daily analyses were performed.

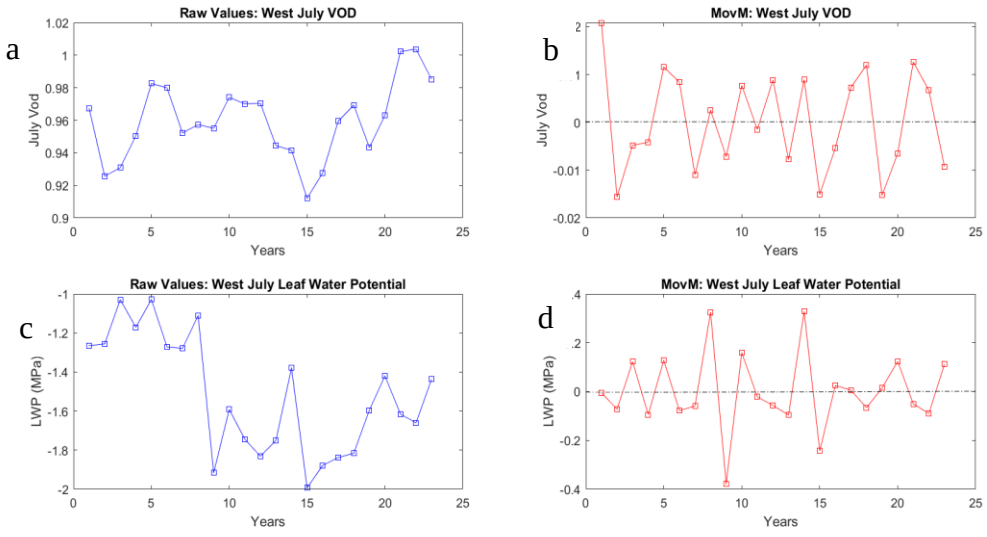

Figure 3: Western site monthly July VOD and leaf water potential. a) and c) shows the raw values of VOD and leaf water potential while b) and d) shows the VOD and leaf water potential after applying the moving mean filter (window width of 3).

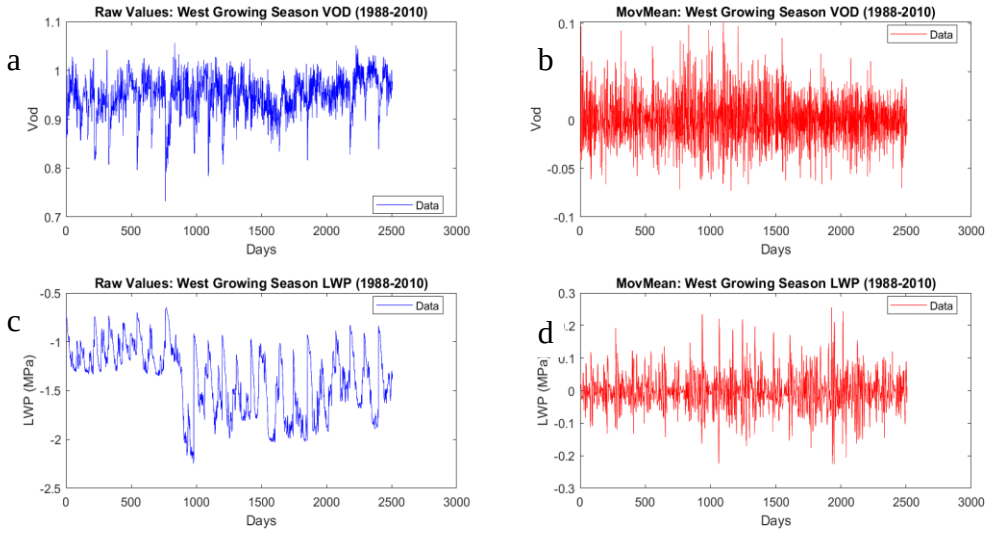

Figure 4: Western site daily growing season VOD and leaf water potential. a) and c) shows the raw values while b) and d) shows the VOD and leaf water potential after applying the moving mean filter (window width of 14).

For the datasets in this research, the statistical test chosen was Spearman's Rho non-parametric test because the VOD, precipitation, vapor pressure deficit, evapotranspiration, and leaf water potential violate the principle of normality which is key to performing a parametric test. So instead, the non-parametric version of the Pearson's Rho which is the Spearman's Rho was chosen. The key thing to keep in mind about non-parametric tests is that the inferences they make are not as strong as compared to parametric tests because they do not make as many assumptions about the dataset as parametric tests do.

3.3.2 Monthly Analysis

To investigate the association between VOD and the chosen variables, the monthly correlations were first considered to examine the long-term patterns and how it follows the seasonal trends.
In executing the correlation test, the target period was the growing season because the forest is deciduous. Hence, care had to be taken to avoid the very beginning of the growing and senescence stage because these have the potential of introducing a lot of noise into the analysis.

For the eastern site, Jones et al. (2012) found the VOD start of the growing season to be between 1st and 15th March which coincided with the NDVI Greenup date. The end of season estimates which is in November was taken from the United States Geological Survey phenology viewer (https://phenology.cr.usgs.gov/viewer/). To ensure that we capture accurately a time that leaves were on trees, the growing season for this site was marked from 15th May to 31st August. The growing season for the western site however was pegged at 1st July to 30th September following the NDVI greenness seasonality of the site obtained from SPOT Vegetation data (ESA CCI-LC 2017).

The Spearman Rho test and its p-value were used to test the strength of correlation between the VOD of each month in the growing season against its corresponding temperature, precipitation, vapor pressure deficit, evapotranspiration, and leaf water potential. The relationship was fitted with a cubic curve to obtain the R^2 and root mean square error (RMSE). It is well known that climate influences vegetation growth and dynamics (Nemani et al. 2003), but vegetation reaction to climate is often complex and with temporal effects (Anderegg et al. 2015). Precisely, the climatic conditions of a particular previous month or months could affect the vegetation growth signally, characterizing the time-lag effect (Wu et al., 2015 as cited in Ding et al. 2020). To test for lags, it is important to know the climate and vegetation composition of the region. For both the eastern and western sites, Ding et al. (2020) found that for temperature there was no time effect for the regions, but it had a one-month accumulation effect. Time accumulation refers to the scenario where vegetation growth is distinctly affected by the cumulative climate conditions of the previous month/s plus the current month (Vicente-Serrano et al. 2013). In terms of precipitation for the study regions, Ding et al. (2020), also determined a two-month lag and a one-month accumulation effect.

Therefore, temperature lags were tested for the previous one month and the current month, and the same was done for vapor pressure deficit since it is strongly influenced by temperature. Precipitation lags were tested with the previous two months and current month data. The Spearman Rho coefficient, p-value, $R^{2,}$ and RMSE were also computed for the individual growing season month lags.

3.3.3 Daily Analysis

With the monthly analyses testing for correlations over relatively long-time intervals, the daily analyses sought to investigate the short-term variations in VOD following the daily alterations of temperature, precipitation, vapor pressure deficit, evapotranspiration, and leaf water potential. On this basis, the daily data for each year's growing season was concatenated together to form a single time series for each variable for the entire study period.

Univariate correlations with VOD were done on temperature, precipitation, vapor pressure deficit, evapotranspiration, and leaf water potential. The next step was to test for the influence of two predictors on VOD in multiple regression. The rationale behind this was to investigate whether two variables can/may provide better explanatory power to VOD than the singular correlations. So, temperature and precipitation, precipitation and vapor pressure deficit, temperature and vapor pressure deficit were tested in that fashion and order on VOD. The R^2, adjusted R^2, p-value, and RMSE were computed. What the adjusted R^2 does is to determine whether adding another predictor to the model improves it or not.

3.3.4 Hydraulic Strategy Analysis

To investigate the hydraulic strategy of the different PFTs, the five PFTs (10,12, 15, 16, and 22) used in this study were analyzed in a boxplot. These PFTs represent the opposite sides of the isohydricity spectrum. PFTs 10, 12, and 15 on the right side of the spectrum representing conservative strategy, and PFTs 16 and 22 on the left side of the spectrum, representing risk-taking strategy (see figure 1). The relatively conservative

PFTs invest in building wood density and a resilient hydraulic regime while the relatively risk-taking PFTs prioritize carbon capture and thus higher leaf area.
The absolute daily growing season leaf water potential from 2000 to 2010 for each year was averaged to create a singular daily time-series for each of the PFTs and study site. The unfiltered daily growing season leaf water potential for the five PFTs and study sites was plotted. However, to explore the explanatory power, PFTs 10 and 22 were used. The designated growing season for each study site was filtered using the moving mean (window width 14) and regressed against VOD. The Spearman Rho coefficient, p-value, R^2, and RMSE are also presented.

4 Results

4.1 Testing Meteorological Variables

4.1.1 Monthly Correlations

Table 3: Eastern site monthly growing season regression analysis. Determination of the Spearman Rho coefficient, p-value, R^2, and RMSE for temperature (TMP), vapor pressure deficit (VPD), and precipitation (PRE) against VOD. Lags tested for TMP, VPD and PRE. Asterisks indicate significant values.

	May				**June**				**July**				**August**			
	Rho	*pVal*	R^2	*rmse*	*Rho*	*pVal*	R^2	*rmse*	*Rho*	*pVal*	R^2	*rmse*	*Rho*	*pVal*	R^2	*rmse*
TMP	-0.8 *	0 *	0.72	0.07	-0.6 *	0 *	0.36	0.07	-0.6 *	0.002 *	0.32	0.06	-0.8 *	0 *	0.71	0.05
Lag	-0.6 *	0 *	0.51	0.1	-0.3	0.1	0.23	0.1	-0.6 *	0.004 *	0.27	0.06	-0.8 *	0 *	0.77	0.04
VPD	-0.3	0.2	0.17	0.1	0.1	0.06	0.09	0.1	0.1	0.7	0.19	0.06	0.3	0.2	0.4	0.08
Lag	-0.4	0.1	0.28	0.1	0.04	0.8	0.1	0.1	0.1	0.7	0.35	0.06	0.5 *	0.01 *	0.32	0.08
PRE	0.1	0.6	0.24	0.1	0.1	1	0.05	0.1	0.2	0.4	0.1	0.07	0.5 *	0 *	0.34	0.08
Lag	-0.2	0.3	0.15	0.1	0.1	0.6	0.28	0.07	0.2	0.5	0.05	0.07	0.5 *	0 *	0.38	0.08

In Table 3, the results of the monthly growing season correlations for the eastern site are presented. For temperature, the Spearman rho coefficient for May (-0.8) indicates a negative monotonic relationship ($p<0.01$) between VOD and temperature for May, whereby an increase in temperature results in a decrease in VOD and vice versa. The R^2 of 0.72 also implies that 72% of the variation in May VOD can be attributed to variation in May temperature. June and July VOD also have a negative monotonic relationship with their corresponding temperatures and is also statistically significant as evidenced by the p-values of both months. However, June and July have relatively weaker R^2 of 0.36 and 0.32, respectively. In August as well there is evidence of a negative relationship ($p<0.01$) supported by an R^2 of 0.71. Temperature lags for the previous and current months could not provide comparatively a better explanatory power to VOD than the original months. Except in August where the R^2 (0.77) shows a stronger explanatory power relative to the R^2 of the original month.

For VOD and vapor pressure deficit, the relationships are non-significant for all original months, including the lags except for August. In August-lag the vapor pressure deficit provides a significant ($p\leq0.01$) and relatively stronger relationship with VOD.

Original months and lag months precipitation coefficients for May, June, and July are all insignificant ($p>0.05$). However, in August both the original and lag correlations are significant and show a positive relationship with VOD. A positive monotonic relationship here implies that an increase in precipitation will potentially cause an increase in VOD.

Table 4: Western site monthly growing season regression analysis. Determination of the Spearman Rho coefficient, p-value, R^2, and RMSE for temperature (TMP), vapor pressure deficit (VPD), and precipitation (PRE) against VOD. Lags tested for TMP, VPD and PRE. Asterisks indicate significant values.

	July				**August**				**September**			
	Rho	*pVal*	*R^2*	*rmse*	*Rho*	*pVal*	*R^2*	*rmse*	*Rho*	*pVal*	*R^2*	*rmse*
TMP	-0.5 *	0.02 *	0.27	0.04	-0.3	0.2	0.16	0.05	0.4 *	0.04 *	0.15	0.07
Lag	-0.5 *	0.03 *	0.3	0.04	-0.2	0.3	0.1	0.05	0.2	0.3	0.1	0.07
VPD	0.2	0.5	0.05	0.05	0.3	0.2	0.15	0.05	-0.1	0.7	0.21	0.06
Lag	0.3	0.1	0.16	0.05	0.1	0.7	0.02	0.06	0.1	0.8	0.19	0.06
PRE	0.05	0.8	0.14	0.05	0.2	0.4	0.27	0.05	-0.5 *	0.01 *	0.34	0.06
Lag	0.4	0.1	0.21	0.04	-0.2	0.5	0.02	0.06	-0.2	0.4	0.1	0.07

The results of the monthly growing season correlations for the western site are presented in Table 4. For temperature, there is evidence of a negative monotonic relationship ($p = 0.02$) in July and the reverse in September ($p = 0.04$). In August, however, the relationship is nonsignificant. Except for July, temperature lags for the previous and current months relatively did not provide better explanatory power to VOD as they are all nonsignificant.

In the western site, there is no relationship between VOD and vapor pressure deficit for all three months ($p>0.05$). The same holds for the lags as well. For precipitation as well there is statistical insignificance across all months apart from September. September precipitation has a negative relationship with VOD ($p\leq0.01$) and an R^2 of 0.34. In testing precipitation lags, all three months gave statistical insignificance.

4.1.2 Daily Correlations

Table 5: Eastern site daily growing season correlation analysis. Univariate and multiple linear regression of temperature (TMP), precipitation (PRE), vapor pressure deficit (VPD), plant evapotranspiration (ET), and leaf water potential (LWP). Spearman rho coefficient, R^2, adjusted $R^{2,}$ and p-values. Asterisks indicate significant values.

Univariate	**Rho**	**R^2**	***p*Val**
TMP	-0.23 *	0.06	0 *
VPD	0.1 *	0.01	0 *
PRE	-0.07 *	0.01	0.001
Multiple Linear Regression	**R^2**	**Adj R^2**	***p*Val**
TMP Vs PRE	0.06 *	0.1	0 *
PRE Vs VPD	0.029 *	0.03	0 *
TMP Vs VPD	0.06 *	0.06	0 *

In Table 5, the results of the daily growing season univariate and multiple linear regressions for the eastern study area are presented. The univariate and multiple linear correlations of temperature, vapor pressure deficit, and precipitation all show statistical significance but have very weak R^2's, hence little explanatory power. For the univariate, temperature and precipitation have a negative relationship with VOD while vapor pressure deficit has a positive relationship with VOD. The multiple linear regressions did not lead to an increase in explanatory power over the best univariate regression as both the R^2 and adjusted R^2 are very weak in all three combinations of temperature, vapor pressure deficit, and precipitation.

The western study area results for both the univariate and multiple linear regression show no statistical significance for all variables and combinations (see appendix S1).

4.2 Testing Simulated Evapotranspiration and Leaf water potential

Table 6: Eastern site *monthly and daily growing season regression analysis. Determination of the Spearman Rho coefficient, p-value, R^2, and RMSE for evapotranspiration (ET), and leaf water potential (LWP) against VOD. Asterisks indicate significant values.*

	May				**June**				**July**				**August**			
Monthly	*Rho*	*pVal*	*R^2*	*rmse*	*Rho*	*pVal*	*R^2*	*rmse*	*Rho*	*pVal*	*R^2*	*rmse*	*Rho*	*pVal*	*R^2*	*rmse*
ET	-0.6 *	0.005 *	0.45	0.1	-0.6 *	0.004 *	0.26	0.07	-0.6 *	0.001 *	0.56	0.05	-0.7 *	0.0001 *	0.58	0.06
LWP	0.2	0.4	0.06	0.1	0.1	0.8	0.1	0.1	-0.1	0.7	0.03	0.07	0.5	0	0.26	0.08
Daily	**Rho**				**R2**				**pVal**							
ET	0.01				0				0.5							
LWP	0.044				0.004				0.03							

In Table 6 evapotranspiration shows a statistically significant ($p<0.01$) and negative monotonic relationship with VOD for all months at the eastern site. The strongest relationship is however seen in August with a Rho coefficient of -0.7 and an R^2 of 0.58.
However, leaf water potential is nonsignificant across all months except August, where there is an indication of a positive relationship with VOD but a rather weak R^2 of 0.26.
The daily correlation of leaf water potential shows statistical significance but has a very weak R^2, hence little explanatory power. Daily evapotranspiration on the other hand shows no significance with daily VOD. Overall, no relationship is seen in the short term.

Table 7: Western site monthly and daily growing season regression analysis. Determination of the Spearman Rho coefficient, p-value, R^2, and RMSE for evapotranspiration (ET), and leaf water potential (LWP) against VOD. Asterisks indicate significant values.

	July				**August**				**September**			
Monthly	*Rho*	*pVal*	*R^2*	*rmse*	*Rho*	*pVal*	*R^2*	*rmse*	*Rho*	*pVal*	*R^2*	*rmse*
ET	0.3	0.2	0.11	0.05	-0.1	0.7	0.2	0.05	-0.4	0.03	0.28	0.06
LWP	0.3	0.2	0.1	0.05	0.2	0.3	0.24	0.05	-0.2	0.3	0.19	0.06
Daily	**Rho**				**R^2**				**pVal**			
ET	0.1 *				0.01				0.004 *			
LWP	0.003				0				0.9			

Looking at Table 7, plant evapotranspiration shows a negative relationship with VOD in September ($p = 0.03$) but remains nonsignificant in both July and August. Even so, September has a weak R2 of 0.28 which implies that only 28% of the variation in September VOD is explained by variations in its corresponding evapotranspiration. Leaf water potential, on the other hand, displays statistical insignificance ($p>0.05$) across all months compounded by very weak R2. In the daily correlations, despite statistical significance for evapotranspiration, it has a weak explanatory power to VOD evidenced by a Spearman rho coefficient of 0.1 and R2 of 0.01.

4.3 Testing PFT Hydraulic Strategy

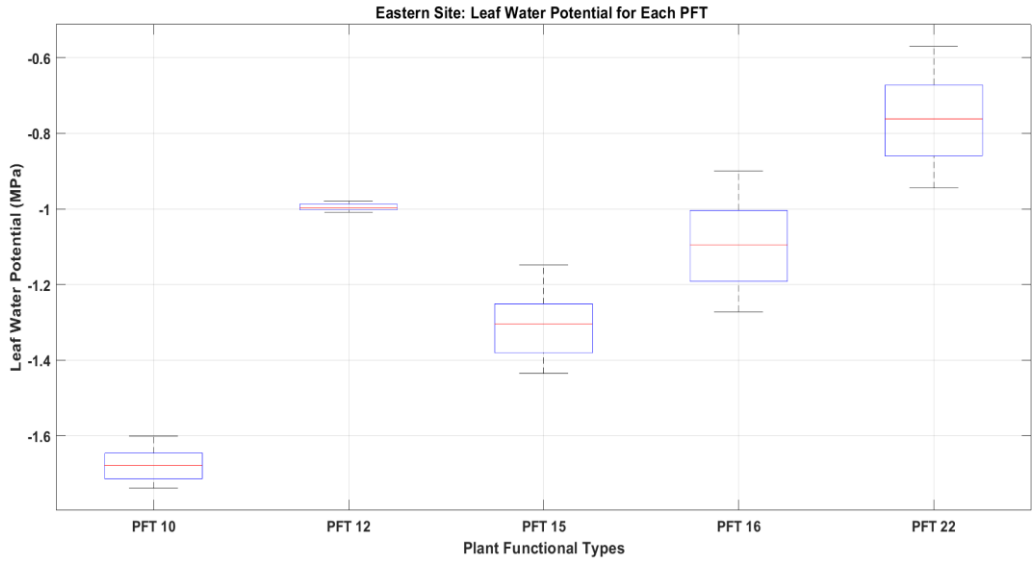

Figure 3: Boxplot showing eastern site growing season leaf water potential for the five plant functional types used in this study, namely PFT 10, 12, 15, 16, and 22.

PFTs 10, 12, and 15 falls on the conservative spectrum of the isohydricity spectrum while PFTs 16 and 22 belong to the risk-taking side. At the eastern site, Figure 3 shows that PFTs 10, 12, and 15 show a relatively less variable leaf water potential throughout the growing season as compared to PFT 16 and 22. However, PFT 12 displays the most uniform leaf water potential throughout the growing season which is almost constant.

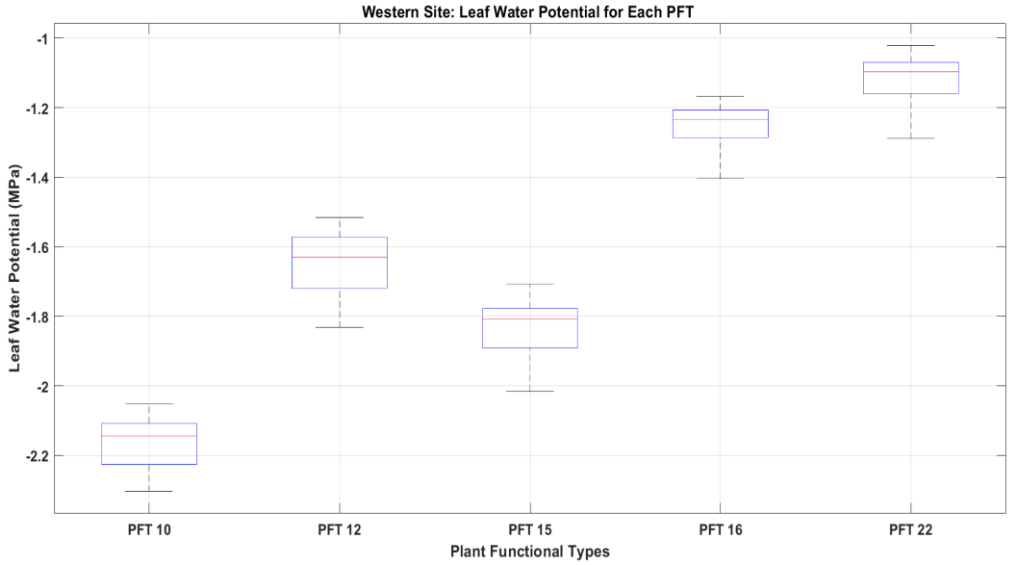

Figure 4: Boxplot showing western site growing season leaf water potential for the five plant functional types used in this study, namely PFT 10, 12, 15, 16, and 22.

At the western site, Figure 4 indicates that PFTs 16, and 22 have a relatively less variable (or almost identical) leaf water potential throughout the growing season as compared to PFT 10, 12, and 15. However, PFT 10, 12, and 15 show a variable leaf water potential where a greater portion of the datasets falls below the median. The longer whiskers at the bottom sides of the plots indicate more variation in leaf water potential at relatively very negative levels.

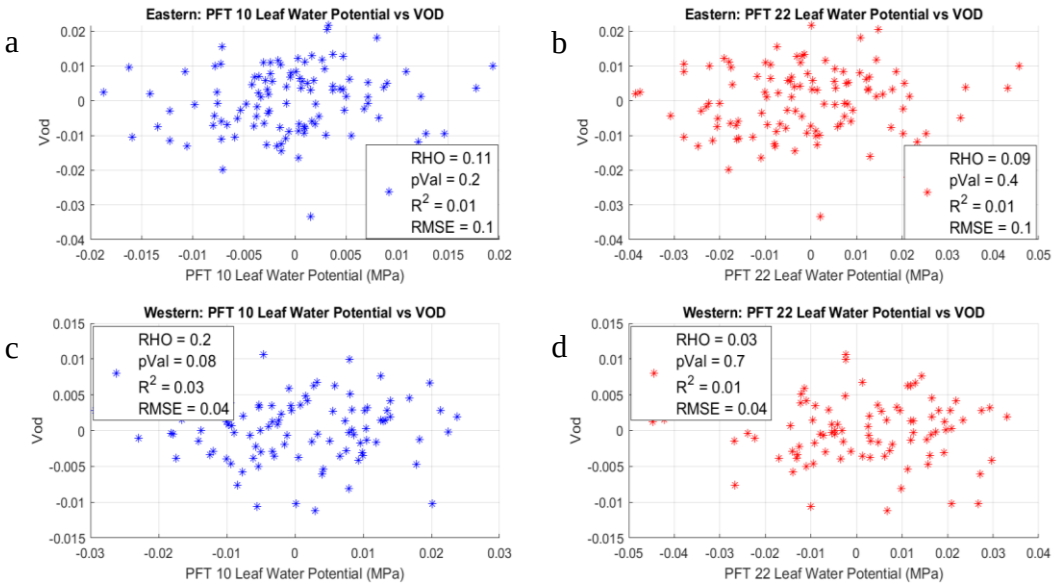

Figure 5: Scatterplots comparing the regression coefficients of the relatively conservative PFT 10 and the relatively risk-taking PFT 22 for the eastern (top – a and b) and western site (bottom – c and d). a) and c) represents PFT 10 and b) and d) stands for PFT 22.

In Figure 5, all four plots show no statistical significance and hence the absence of distinction between the explanatory powers of the two PFTs.

5 Discussion

5.1 To what extent can temporal variability in VOD over broadleaf forests be explained by meteorological variables?

5.1.1 Temperature

Amongst the three meteorological variables tested, temperature appears to have the strongest relationship with VOD for both study sites. At the Eastern site, model results indicate a negative relationship between temperature and VOD for both the monthly and daily correlations. However, the relationship for the growing season months shows a stronger negative correlation for May and August but a comparatively weaker negative correlation for June and July. This may be due to the change in average temperature and precipitation between the growing season months and its effects on the photosynthetic optima of the tree species. Breshears et al. (2005) posit that when elevated temperatures accompany drought, it affects the photosynthetic optima causing a reduction in photosynthesis and impacting both electron transport and rubisco activity (Berry and Bjorkman, 1980; Sage and Kubien, 2007 as cited in McDowell et al. 2008). The average temperature for May, June, July, and August is 15, 20, 22, and 22 °C respectively (see S4), while total monthly precipitation is 90, 88, 93, and 76 mm (S5). The strong relationship in May is deemed to be rising from the first half of May (1st to 14th) which has an average temperature of 14 °C and total precipitation of 53 mm. Comparing these values to the second half of May (16 °C and 93 mm respectively), the significantly low precipitation in the first half amidst rising temperature is considered responsible for amplifying the temperature effect in the second half.

Despite the consistent rise in temperature (May - July), June and July tend to have a weaker relationship with VOD which can be attributed to the abundance in precipitation weakening the influence of temperature on VOD for both months. In August, however, consistently high temperatures coupled with a significant decline in precipitation boosts the relationship between temperature and VOD. It is theorized that this is probably due to the triggering of the hydraulic apparatus of the tree to close its stomata to avoid water loss which in turn diminishes the tree's carbon assimilation. According to Kolb and Sperry (1999), rising temperature coupled with declining precipitation initiates drought which may decrease photosynthesis by mechanisms such as loss of leaf turgor and leaf shedding (Tyree et al 1993 as cited in McDowell et al. 2008) which may invariably cause a decline in VOD. In terms of lags, only August provided an improved explanatory power looking at the R^2. This is quite expected as it combines the higher temperatures of July to that of August which is also high. This further goes to show how rising temperature negatively impacts VOD.

In the western site, the temperature relationship with VOD is only seen in July and September. In September however, a positive relationship is seen which is counter-intuitive. The average temperature for July, August, and September is 16.5, 15, and 11 °C (see S6) respectively and total precipitation is 27, 32, and 28 mm (S7). Once again considering the temperature and precipitation changes, it seems the negative relationship in July is caused by higher temperatures (16.5 °C) and low precipitation (27 mm) which induces stress on trees and decreases VOD (McDowell et al. 2008). September on the other hand has a considerably lower temperature coupled with a higher precipitation level which implies little evaporative demand on tree leaves. As

seen in the eastern site, an abundance of precipitation reduces the temperature effect and thus positively impacting VOD. In checking the lags, only July provided a significant and improved explanatory power to VOD, and this can largely be attributed to the carry-over effect of the higher temperatures (13 °C) and very little precipitation (17 mm) in June compounding the effects of the current month.

5.1.2 Vapor pressure deficit

The monthly vapor pressure deficit for the eastern and western sites shows no statistical significance with VOD for each of the months except for August lag at the eastern site, but the relationship is positive. Moreover, analyzing the short-term variations for the eastern site (table 5), the daily correlations for vapor pressure deficit and VOD also show a positive but weak explanatory power. This positive and weak relationship is unexpected as higher vapor pressure deficit is known to be associated with higher temperatures and decreased hydraulic conductance (Zhang et al. 2017) which reduces water supply to the leaves, thereby affecting VOD negatively (McDowell et al. 2008). This is especially perplexing when August has already been established to have reduced precipitation and sustained higher temperatures. But in hindsight, the August lag for the Eastern site combines the vapor pressure deficit of the previous month (July) which received copious precipitation (93mm) and thus is moisture laden. Critical scrutiny at the relationship between the meteorological variables at the eastern site indicates that, vapor pressure deficit is primarily controlled by precipitation and not temperature (see appendix - S2 and S3). Therefore, this may be the reason why a positive relationship is seen in August lag as well as the daily correlations at the Eastern site.

5.1.3 Precipitation

A statistically significant relationship between precipitation and VOD is only seen in August and September for the eastern and western sites, respectively. Although the short-term daily correlation for the eastern site shows significance, the Rho and R^2 values have little explanatory power and thus no causal relationship can be drawn from it.

August precipitation and lag at the eastern site have a positive relationship with VOD which conforms with our hypothesis and existing literature. Precipitation promotes vegetation growth by aiding higher evapotranspiration which leads to a higher water load in the atmosphere (higher relative humidity) and thus lowering atmospheric water demand (Shaw et al. 2000; Breshears et al. 2005; Macalady and Bugman 2014 as cited in Meddens et al. 2015) and in turn stimulates leaf turgidity which directly increases VOD. On the other hand, the largely nonexistent relationship between precipitation and VOD at the eastern site (May, June, and July) is attributed to the area being so wet that more precipitation does not affect it (Momen et al. 2017). Conversely, it is postulated that the western site is consistently so dry that it is always water limited. September however has a negative relationship with VOD which is counter-intuitive but seems to be caused by an early leaf drop signal (see S8) due to the beginning of autumn. As autumn starts, precipitation will undoubtedly relate negatively to VOD due to the combined effects of leaf drying (loss of turgor) and falling.

Apart from the sites being too wet or too dry, other ecosystem factors such as increased canopy interception, the presence of epiphytes, the bark texture and architecture of stems and trunks, and the rooting depth can enhance, mostly delay or reduce the effects of precipitation (Chapin III et al. 2011).

Canopy interception accounts for 10 to 20 % of precipitation in closed-canopy ecosystems and refers to the portion of precipitation that does not reach the ground (Bonan 2008). The ability of the canopy to intercept and store water depends on the canopy surface area. With the study area species being broadleaves with wide leaf areas, it is a possibility that canopy interception could be increasing VOD directly after rainfall events (before the water on the leaves and stems evaporate) while reducing the impacts of precipitation on VOD on a longer timescale (weeks to months), by limiting the amount of water which reaches the soil and is therefore available for root uptake. Chapin III et al. (2011) noted that a proportion of precipitation evaporates and returns directly to the atmosphere without reaching the soil through the mechanisms of canopy interception, especially after a light rain.

Epiphytes which are rooted in the canopy are angiosperms that grow on other plants and derive their moisture and nutrient from them. The presence of epiphytes increases canopy interception as that is their source of water supply and factors such as epiphyte load and stand age may pose a far greater influence on canopy interception (Chapin III et al. 2011) by reducing the water that reaches the soil and thus the water the tree receives.

Moreover, Waring and Running (2007) explain that the texture of the bark of the tree, as well as the structure of the stems and trunks, also dictates the amount and direction of stemflow whereby trees with smoother barks (12 % of precipitation) have more stemflow and hence more water reaching the soil than trees with rough or textured backs (2% of precipitation).

The rooting depth of tree species has key ecosystem repercussions because it determines the soil volume that is exploited by vegetation. Specie-specific differences in rooting depth determine the variability in water supply and drought stress. Temperate deciduous species have been found to have relatively shallower vertical rooting depth (below 5 meters) as compared to conifers (Chapin III et al. 2011).

From the above analysis, it is suggested that the greater lack of correlation between VOD and precipitation could be a mixture of interacting factors ranging from the wetness or dryness of the area to the physiological traits of the tree species under study.

5. 2 Does a process-based simulation of evapotranspiration and leaf water potential provide a better explanation of VOD than raw meteorological variables?

5.2.1 Evapotranspiration

To answer the second research question, the following was discovered. On a longer timescale (monthly) evapotranspiration is determined to relate strongly with VOD but less robustly than the temperature at the eastern site, but does not influence on a shorter timescale (daily). Meanwhile, at the western site, evapotranspiration has a relationship with VOD only in September with little to no explanatory power on a shorter timescale. Therefore, the simulated variables do not provide added skill over the raw meteorological variables (mostly temperature). This may be because there is no relationship in reality or because the model does not simulate these well, or there is a scale mismatch.

The rate of plant evapotranspiration, as well as the direction of influence, is dependent on the vegetation growth stage, its characteristics, and soil moisture levels (Wang et al. 2012; Zhang et al. 2015; Pei et al. 2017; Liu et al. 2019). The inverse relationship between evapotranspiration and VOD at both sites conflicts with literature because, in the growing season, rising temperature and precipitation promote vegetation growth and density and cause increases in evapotranspiration levels (Kramer et al. 2015; Zhang et al. 2015; Pei et al. 2017). Thus, increasing vegetation growth, causes VOD levels to rise which should theoretically induce more evapotranspiration, leading to a positive relationship. But a negative relationship is rather evident and prompted a look at the relationship between precipitation and evapotranspiration at each site.

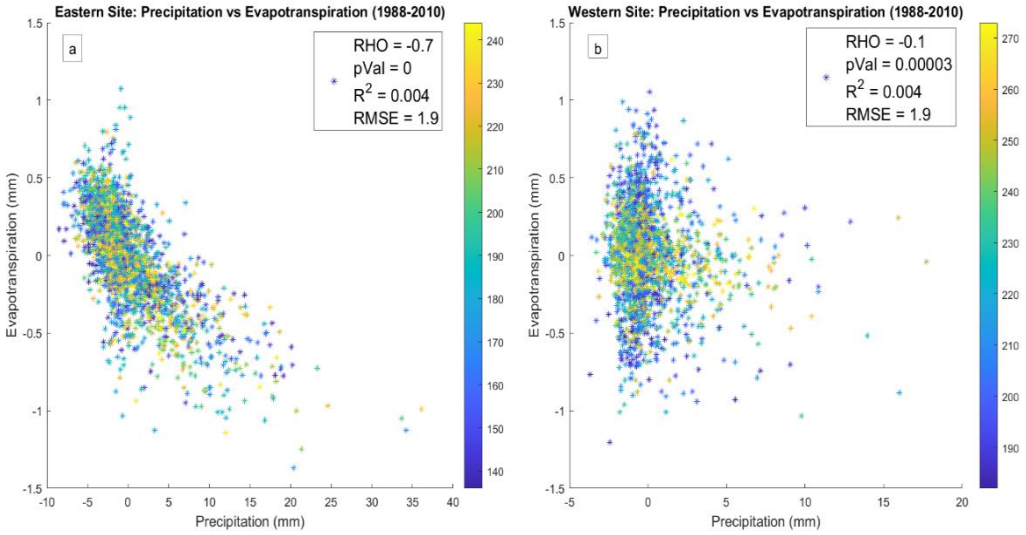

Figure 6: Daily precipitation against evapotranspiration. The axes are normalized to the mean of zero. Plot (a) for the eastern site and plot (b) for the western site.

Figure 6 shows that at the eastern site there is a very strong negative relationship between precipitation and evapotranspiration as well as the western site. In looking at the factors that might cause such a relationship, water is indeed needed for evapotranspiration to occur, but high evapotranspiration also requires high demand from the atmosphere (i.e., low vapor pressure deficit). Rainy conditions are cloudy, with low insolation and high relative humidity and therefore a high vapor pressure deficit. So, rain might promote evapotranspiration in the medium to long term but reduce it in the short term (as shown in figure 6). Overall, the relationship between precipitation and evapotranspiration is complex and governed by several aspects ranging from the magnitude of atmospheric demand to the availability of water, and stomatal conductance, amongst others (Wang et al. 2012; Zhang et al. 2015; Pei et al. 2017; Liu et al. 2019). It is deemed that the experimental LPJ-GUESS model being used here is deficient in capturing the dynamics of evapotranspiration at the study regions, however, in both sites a complex relationship over time is likely. Probable areas of additional inquiries are the annual variation of evapotranspiration, the differences between wet and dry periods, the dynamics at each plant developmental stage as well as the ability of the soil to store water. Further probe on evapotranspiration is therefore needed to gain an in-depth understanding of the dynamics and controls at each site.

5.2.2 Leaf water potential

In answering the ability of leaf water potential to provide a better explanation to VOD, it performed unsatisfactorily. At the eastern site (table 6), a significant relationship is only seen in August meanwhile the daily correlation provides statistical significance but holds a negligible explanatory power. The western site however has no relationship with VOD across all three growing season months (table 7) as well as the daily correlations.

Even though both evapotranspiration and leaf water potential combine the demand and supply aspect of water dynamics, leaf water potential is considered a strong predictor of VOD, because it relates more closely to the hydraulic status of plant species and is strongly connected to stomatal closure and xylem embolism (Jarvis, 1976; Sperry and Tyree 1988 as cited in Momen et al. 2017) which characterizes the hydraulic strategies of species. Leaf water potential is influenced by evapotranspiration and the physiological mechanisms trees adopt to avoid exceeding critical limits of evapotranspiration. At higher temperatures, evapotranspiration levels rise, generating tension that sucks up water from the soil to the crown to replenish lost water and photosynthesize and hydrate plant tissues. Thus, evapotranspiration creates a tension difference between the leaf (leaf water potential) and the soil (soil water potential) regulated by the leaf hydraulic conductance (McDowell et al. 2008). To avoid reaching the upper limit of evapotranspiration (which is species-specific), isohydric species will regulate their stomates accordingly, but also face reductions in carbon assimilation causing carbon starvation. Anisohydric species on the other hand do not subvert evapotranspiration from rising excessively, it reaches critical limits which causes a fall in hydraulic conductance due to air entering the xylem conduit. This causes embolism which halts water movement and may lead to hydraulic failure.

In August at the eastern site, a relationship becomes apparent as temperature rises and precipitation falls, triggering the plant senses to regulate stomatal conductance to avert excessive water loss and cavitation as it becomes relatively drier. This indicates a more relatively isohydric strategy which is absent in May, June, and July due to abundant precipitation and relatively cooler temperatures.

In contrast to the strong relationship found between VOD and leaf water potential in Momen et al. (2017), no relationship could be found here. This might be due to model deficiencies in modeling leaf water potential since Momen et al. (2007) used an observational leaf water potential dataset. Moreover, they used predawn leaf water potential while this study used midday leaf water potential. What has not been proven here is the capability of the model to simulate efficiently leaf water potential (which good correlations would have supported). But as explained above, the lack of a correlation can be more multiple reasons, which requires more work such as the incorporation and parameterizing of more defining environmental, physiological, and biological traits into the model to refine outputs as well as testing different processing and analysis techniques.

5.3 Is the explanatory power affected by the hydraulic strategy of the simulated vegetation?

In response to the third research question, a clear link could not be established between the hydraulic strategy of the simulated vegetation and its explanatory power. This is because, at the eastern site, both PFTs 10 and PFT 22 (figure 5) have almost the same Rho and R^2 values. However, the absolute leaf water potential values of the relatively conservative PFTs 10, 12, and 15 show a less variable leaf water potential throughout the growing season as compared to the relatively risk-taking PFTs of 16 and 22 (figure 3). In terms of displaying plant strategy, PFT 12 shows the most isohydric behavior, followed by PFT 10 because they vary much less and are very uniform. PFTs 16 and 22 on the other hand, show a comparatively wider range of leaf water potentials across the growing season and this is cognizant of anisohydric species. However, the difference in the absolute values is unexpected because relatively isohydric species regulate stomatal conductance to prevent leaf water potential from falling, while relatively anisohydric species maintain higher stomatal conductance effectively allowing leaf water potential to fall (lower than isohydric) with declining soil water potential (Momen et al. 2017). Therefore, this is probably due to the model default measurement as PFTs 16 and 22 might not exist in the study grid cells.

On the other hand, the western site seems to show some level of contrast between PFT 10 and PFT 22 (see figure 5), but the relationship is nonsignificant and thus may be purely coincidental. In figure 4, a clear pattern cannot be established amongst the five PFTs as the variations are identical, but the absolute values again suggest the probable nonexistence of PFTs 16 and 22 in the grid cells as they are too high (thus model default measurements).

In comparing the eastern and western plots and distribution, the western site has more variation and spread as compared to the eastern site and this is thought to be a result of the moisture differences between the two sites. Eastern is moisture-laden and thus stress is less daunting while the western site is relatively drier and moisture deficient. It is asserted that due to the abundant moisture content at the eastern site, the specie specific hydraulic strategy does not stand out as the trees are not stressed for water (Konings and Gentine 2017). Conversely, the drier condition of the western site induces more variation and activates the different hydraulic strategies of the tree species and that is why some level of distinction is seen here, but the results are not clear enough to support a definitive conclusion.

5.4 Limitations

One of the key limitations of this study is mixed grid cells, as it was nearly impossible to obtain grid cells with 100% deciduous broadleaf coverage in the observations. This reduces the accuracy of the analysis performed against such VOD signals considering conifers have not yet been parameterized in the experimental version of the LPJ-GUESS model used in this study. Even so, the western site was most affected with more influence from needleleaf and permanently frozen grounds (ice). Another key issue is the gaps that came with the VOD data and the method used in filling those gaps. A simple data filling method was used where the missing value of one day was replaced with that of the previous day. Although this is supported by literature (Moesinger et al. 2020) it can very much wipe out informative daily variations. Again, the lack of

complete knowledge about the specific type, characteristics, and distribution of plant species or land cover for that matter in each sampled grid cell poses a restraint on the depth of discussion or associations that can be made with the results. Similarly, knowledge about the physical environment in which the grid cell exists such as the topography, soil type, depth, and texture could have helped in a stronger disentanglement of the controls on VOD. As McDowell et al. (2008) noted that fine-textured soils have lower hydraulic conductance relative to coarse-textured soils which affect evapotranspiration rates. Deep soils are also found to store winter precipitation for later use in summer whereas shallow soils lose winter precipitation to runoff due to lack of such storage capabilities (Flint and Flint 2012b as cited in van Mantgem et al. 2013). As always with more time, several combinations of associations and lags could have been tested and more factors could have been investigated.

6 Conclusions

Vegetation optical depth is increasingly being used in vegetation studies ranging from phenological to tree mortality studies due to its global coverage and accessibility. To evaluate VOD, this research used climatic variables and chiefly a process-based simulation of evapotranspiration and leaf water potential by the experimental version of LPJ-GUESS. Climate model results indicate a stronger influence of temperature on VOD, followed by precipitation and then vapor pressure deficit. More often a combined influence of temperature and precipitation was seen. Process-based simulation of evapotranspiration and leaf water potential could not provide a relatively better correlation with VOD despite being more directly linked to plant water dynamics and this is linked to model deficiencies. Nonetheless, evapotranspiration performed better in comparison to leaf water potential. In dissecting the explanatory power of the simulated vegetation, some level of variation exists between the PFTs, but no definitive patterns could be deduced from it. At the eastern site though, August consistently had statistical significance, and this is thought to be due to the advancement in the growing season where the temperature is relatively higher and precipitation lower, inducing tree stress.

Analyses of the results show that VOD signals may be simple but the mechanisms that lead to the turgidity or wilting of tree structures are very complex. So much so that, a single variable or mechanism could not suffice satisfactorily in representing the VOD signals and thus tree mortality. Factors such as tree density, tree size, basal area, patch structure, genotype, slope, terrain, presence of pathogens such as bark beetles all play a role. So consequently, a deep understanding of what controls exist in what location and how they interact is key in dissecting VOD signals, understanding mortality, and parameterizing ecosystem models for better reproduction and forecasting of mortality scenarios.

Future studies should aim to replicate the study in a smaller domain and timescale, where extensive information about the location is known, including the kind of controls that exist and how they interrelate. Apart from looking at the controls, future research should also examine critically the relationship between evapotranspiration and VOD as the results of this study (at the eastern site) indicates that it has a great potential of explaining variations in VOD.

7 References

Anderegg, W. R. L., C. Schwalm, F. Biondi, J. J. Camarero, G. Koch, M. Litvak, K. Ogle, J. D. Shaw, et al. 2015. Pervasive drought legacies in forest ecosystems and their implications for carbon cycle models. *Science* 349: 528. doi:10.1126/science.aab1833.

Arend, M., R. M. Link, R. Patthey, G. Hoch, B. Schuldt, and A. Kahmen. 2021. Rapid hydraulic collapse as cause of drought-induced mortality in conifers. *Proceedings of the National Academy of Sciences* 118. National Academy of Sciences. doi:10.1073/pnas.2025251118.

Bastos, A., R. Orth, M. Reichstein, P. Ciais, N. Viovy, S. Zaehle, P. Anthoni, A. Arneth, et al. 2021. Increased vulnerability of European ecosystems to two compound dry and hot summers in 2018 and 2019. *Earth System Dynamics Discussions* 2021: 1–32. doi:10.5194/esd-2021-19.

Beaudoing, H. K., M. Rodell, and B. Li. 2021. GLDAS CLM Land Surface Model L4 daily 0.25 x 0.25 degree V2.0. In . Greenbelt, Maryland, USA: Goddard Earth Sciences Data and Information Services Center (GES DISC). doi:10.5067/LYHA9088MFWQ.

Bigler, C., and T. Veblen. 2011. Changes in litter and dead wood loads following tree death beneath subalpine conifer species in northern Colorado. *Canadian Journal of Forest Research* 41: 331–340. doi:10.1139/X10-217.

Bonan, G. B. 2008. *Ecological Climatology: Principles and Applications*. 2nd ed. Cambridge: Cambridge University Press.

Breshears, D. D., and C. D. Allen. 2002. The importance of rapid, disturbance-induced losses in carbon management and sequestration. *Global Ecology and Biogeography* 11. John Wiley & Sons, Ltd: 1–5. doi:10.1046/j.1466-822X.2002.00274.x.

Breshears, D. D., N. S. Cobb, P. M. Rich, K. P. Price, C. D. Allen, R. G. Balice, W. H. Romme, J. H. Kastens, et al. 2005. Regional vegetation die-off in response to global-change-type drought. *Proceedings of the National Academy of Sciences* 102. National Academy of Sciences: 15144–15148. doi:10.1073/pnas.0505734102.

Brodribb, T. J., D. J. M. S. Bowman, S. Nichols, S. Delzon, and R. Burlett. 2010. Xylem function and growth rate interact to determine recovery rates after exposure to extreme water deficit. *New Phytologist* 188. John Wiley & Sons, Ltd: 533–542. doi:10.1111/j.1469-8137.2010.03393.x.

Chapin III, F. S., P. A. Matson, and P. Vitousek. 2011. *Principles of Terrestrial Ecosystem Ecology*. 2nd ed. Springer-Verlag New York.

Colorado State Forest Service. 2021. Colorado's Major Tree Species. *Colorado's Major Tree Species*.

Cook, B. I., T. R. Ault, and J. E. Smerdon. 2015. Unprecedented 21st century drought risk in the American Southwest and Central Plains. *Science Advances* 1: e1400082. doi:10.1126/sciadv.1400082.

Deloire, A., and D. Heyns. 2011. The Leaf Water Potentials: Principles, Method and Thresholds. *WineLand Media*.

Ding, Y., Z. Li, and S. Peng. 2020. Global analysis of time-lag and -accumulation effects of climate on vegetation growth. *International Journal of Applied Earth Observation and Geoinformation* 92: 102179. doi:10.1016/j.jag.2020.102179.

Fisher, R. A., C. D. Koven, W. R. L. Anderegg, B. O. Christoffersen, M. C. Dietze, C. E. Farrior, J. A. Holm, G. C. Hurtt, et al. 2018. Vegetation demographics in Earth System Models: A review of progress and priorities. *Global Change Biology* 24: 35–54. doi:https://doi.org/10.1111/gcb.13910.

Frankson, R., Kenneth. E. Kunkel, L. Stevens, and D. Easterling. 2017. *Colorado State Climate Summary*. NOAA Technical Report.

Frappart, F., J.-P. Wigneron, X. Li, X. Liu, A. Al-Yaari, L. Fan, M. Wang, C. Moisy, et al. 2020. Global Monitoring of the Vegetation Dynamics from the Vegetation Optical Depth (VOD): A Review. *Remote Sensing* 12. doi:10.3390/rs12182915.

Fu, X., and F. C. Meinzer. 2019. Metrics and proxies for stringency of regulation of plant water status (iso/anisohydry): a global data set reveals coordination and trade-offs among water transport traits. *Tree Physiology* 39: 122–134. doi:10.1093/treephys/tpy087.

Griffith, D. M., and R. H. Widmann. 2003. *Forest Statistics for West Virginia:1989 and 2000*. Resource Bulletin NE-157. Newtown Square: Forest Service - USDA.

Hammond, W. M., K. Yu, L. A. Wilson, R. E. Will, W. R. L. Anderegg, and H. D. Adams. 2019. Dead or dying? Quantifying the point of no return from hydraulic failure in drought-induced tree mortality. *New Phytologist* 223: 1834–1843. doi:https://doi.org/10.1111/nph.15922.

Hickler, T., B. Smith, M. T. Sykes, M. B. Davis, S. Sugita, and K. Walker. 2004. Using a Generalized Vegetation Model to Simulate Vegetation Dynamics in Northeastern USA. *Ecology* 85. Ecological Society of America: 519–530. JSTOR.

Hickler, T., I. C. Prentice, B. Smith, M. T. Sykes, and S. Zaehle. 2006. Implementing plant hydraulic architecture within the LPJ Dynamic Global Vegetation Model. *Global Ecology and Biogeography* 15: 567–577. doi:https://doi.org/10.1111/j.1466-8238.2006.00254.x.

Hoffmann, W., R. Marchin, P. ABIT, and O. L. Lau. 2011. Hydraulic failure and tree dieback are associated with high wood density in a temperate forest under extreme drought. *Global Change Biology* 17: 2731–2742. doi:10.1111/j.1365-2486.2011.02401.x.

Holdridge, L. R. 1967. *Life zone ecology*. (rev. ed.). San Jose, Costa Rica: Tropical Science Center.

Joetzjer, E., H. Douville, C. Delire, and P. Ciais. 2013. Present-day and future Amazonian precipitation in global climate models: CMIP5 versus CMIP3. *Climate Dynamics* 41: 2921–2936. doi:10.1007/s00382-012-1644-1.

Jones, M. O., L. A. Jones, J. S. Kimball, and K. C. McDonald. 2011. Satellite passive microwave remote sensing for monitoring global land surface phenology. *Remote Sensing of Environment* 115: 1102–1114. doi:10.1016/j.rse.2010.12.015.

Jones, M. O., J. S. Kimball, L. A. Jones, and K. C. McDonald. 2012. Satellite passive microwave detection of North America start of season. *Remote Sensing of Environment* 123: 324–333. doi:10.1016/j.rse.2012.03.025.

Jupp, T. E., P. M. Cox, A. Rammig, K. Thonicke, W. Lucht, and W. Cramer. 2010. Development of probability density functions for future South American rainfall. *The New phytologist* 187. England: 682–693. doi:10.1111/j.1469-8137.2010.03368.x.

Kolb, K. J., and J. S. Sperry. 1999. Differences in Drought Adaptation between Subspecies of Sagebrush (Artemisia Tridentata). *Ecology* 80. Ecological Society of America: 2373–2384. JSTOR. doi:10.2307/176917.

Konings, A. G., and P. Gentine. 2017. Global variations in ecosystem-scale isohydricity. *Global Change Biology* 23. John Wiley & Sons, Ltd: 891–905. doi:10.1111/gcb.13389.

Konings, A. G., M. Piles, K. Rötzer, K. A. McColl, S. K. Chan, and D. Entekhabi. 2016. Vegetation optical depth and scattering albedo retrieval using time series of dual-polarized L-band radiometer observations. *Remote Sensing of Environment* 172: 178–189. doi:https://doi.org/10.1016/j.rse.2015.11.009.

Kramer, R. J., L. Bounoua, P. Zhang, R. E. Wolfe, T. G. Huntington, M. L. Imhoff, K. Thome, and G. L. Noyce. 2015. Evapotranspiration Trends Over the Eastern United States During the 20th Century. *Hydrology* 2: 93–111. doi:10.3390/hydrology2020093.

Liu, R., J. Wen, X. Wang, Z. Wang, Z. Li, Y. Xie, L. Zhu, and D. Li. 2019. Derivation of Vegetation Optical Depth and Water Content in the Source Region of the Yellow River using the FY-3B Microwave Data. *Remote Sensing* 11. doi:10.3390/rs11131536.

Liu, Y. Y., A. I. J. M. van Dijk, R. A. M. de Jeu, J. G. Canadell, M. F. McCabe, J. P. Evans, and G. Wang. 2015. Recent reversal in loss of global terrestrial biomass. *Nature Climate Change* 5: 470–474. doi:10.1038/nclimate2581.

M. Vreugdenhil, W. A. Dorigo, W. Wagner, R. A. M. de Jeu, S. Hahn, and M. J. E. van Marle. 2016. Analyzing the Vegetation Parameterization in the TU-Wien ASCAT Soil Moisture Retrieval. *IEEE Transactions on Geoscience and Remote Sensing* 54: 3513–3531. doi:10.1109/TGRS.2016.2519842.

van Mantgem, P. J., J. C. B. Nesmith, M. Keifer, E. E. Knapp, A. Flint, and L. Flint. 2013. Climatic stress increases forest fire severity across the western United States. *Ecology Letters* 16: 1151–1156. doi:https://doi.org/10.1111/ele.12151.

McDowell, N., W. T. Pockman, C. D. Allen, D. D. Breshears, N. Cobb, T. Kolb, J. Plaut, J. Sperry, et al. 2008. Mechanisms of plant survival and mortality during drought: why do some plants survive while others succumb to drought? *New Phytologist* 178. John Wiley & Sons, Ltd: 719–739. doi:10.1111/j.1469-8137.2008.02436.x.

McDowell, N. G., D. J. Beerling, D. D. Breshears, R. A. Fisher, K. F. Raffa, and M. Stitt. 2011. The interdependence of mechanisms underlying climate-driven vegetation mortality. *Trends in Ecology & Evolution* 26: 523–532. doi:10.1016/j.tree.2011.06.003.

Meddens, A. J. H., J. A. Hicke, A. K. Macalady, P. C. Buotte, T. R. Cowles, and C. D. Allen. 2015. Patterns and causes of observed piñon pine mortality in the southwestern United States. *New Phytologist* 206: 91–97. doi:https://doi.org/10.1111/nph.13193.

Moesinger, L., W. Dorigo, R. De Jeu, R. Van der Schalie, T. Scanlon, I. Teubner, and M. Forkel. 2019. The Global Long-term Microwave Vegetation Optical Depth Climate Archive VODCA (Version 1.0). *Zenodo*. doi:doi:10.5281/zenodo.2575599.

Moesinger, L., W. Dorigo, R. de Jeu, R. van der Schalie, T. Scanlon, I. Teubner, and M. Forkel. 2020. The global long-term microwave Vegetation Optical Depth Climate Archive (VODCA). *Earth System Science Data* 12: 177–196. doi:10.5194/essd-12-177-2020.

Momen, M., J. D. Wood, K. A. Novick, R. Pangle, W. T. Pockman, N. G. McDowell, and A. G. Konings. 2017. Interacting Effects of Leaf Water Potential and Biomass on Vegetation Optical Depth. *Journal of Geophysical Research: Biogeosciences* 122. John Wiley & Sons, Ltd: 3031–3046. doi:10.1002/2017JG004145.

Nabais, C., J. Hansen, R. David-Schwartz, M. Klisz, R. López, and P. Rozenberg. 2018. The effect of climate on wood density: What provenance trials tell us? *Forest Ecology and Management* 408: 148–156. doi:10.1016/j.foreco.2017.10.040.

Nemani, R. R., C. D. Keeling, H. Hashimoto, W. M. Jolly, S. C. Piper, C. J. Tucker, R. B. Myneni, and S. W. Running. 2003. Climate-Driven Increases in Global Terrestrial Net Primary Production from 1982 to 1999. *Science* 300: 1560. doi:10.1126/science.1082750.

Papastefanou, P., C. S. Zang, T. A. M. Pugh, D. Liu, T. E. E. Grams, T. Hickler, and A. Rammig. 2020. A Dynamic Model for Strategies and Dynamics of Plant Water-Potential Regulation Under Drought Conditions. *Frontiers in Plant Science* 11: 373. doi:10.3389/fpls.2020.00373.

Park Williams, A., C. D. Allen, A. K. Macalady, D. Griffin, C. A. Woodhouse, D. M. Meko, T. W. Swetnam, S. A. Rauscher, et al. 2013. Temperature as a potent driver of regional forest drought stress and tree mortality. *Nature Climate Change* 3: 292–297. doi:10.1038/nclimate1693.

Pei, T., X. Wu, X. Li, Y. Zhang, F. Shi, Y. Ma, P. Wang, and C. Zhang. 2017. Seasonal divergence in the sensitivity of evapotranspiration to climate and vegetation growth in the Yellow River Basin, China. *Journal of Geophysical Research: Biogeosciences* 122: 103–118. doi:https://doi.org/10.1002/2016JG003648.

Powell, T. L., D. R. Galbraith, B. O. Christoffersen, A. Harper, H. M. A. Imbuzeiro, L. Rowland, S. Almeida, P. M. Brando, et al. 2013. Confronting model predictions of carbon fluxes with measurements of Amazon forests subjected to experimental drought. *New Phytologist* 200. John Wiley & Sons, Ltd: 350–365. doi:10.1111/nph.12390.

Rao, K., W. R. L. Anderegg, A. Sala, J. Martínez-Vilalta, and A. G. Konings. 2019. Satellite-based vegetation optical depth as an indicator of drought-driven tree mortality. *Remote Sensing of Environment* 227: 125–136. doi:10.1016/j.rse.2019.03.026.

Reich, P. B. 2014. The world-wide 'fast–slow' plant economics spectrum: a traits manifesto. *Journal of Ecology* 102. John Wiley & Sons, Ltd: 275–301. doi:10.1111/1365-2745.12211.

Rowland, L., A. Costa, D. Galbraith, R. Oliveira, O. Binks, A. Oliveira, A. Pullen, C. Doughty, et al. 2015. Death from drought in tropical forests is triggered by hydraulics not carbon starvation. *Nature* 528. doi:10.1038/nature15539.

Runkle, J., K. E. Kunkel, R. Frankson, and B. C. Stewart. 2017. *West Virginia State Climate Summary*.

Schuldt, B., A. Buras, M. Arend, Y. Vitasse, C. Beierkuhnlein, A. Damm, M. Gharun, T. E. E. Grams, et al. 2020. A first assessment of the impact of the extreme 2018 summer drought on Central European forests. *Basic and Applied Ecology* 45: 86–103. doi:10.1016/j.baae.2020.04.003.

Smith, B., D. W\aarlind, A. Arneth, T. Hickler, P. Leadley, J. Siltberg, and S. Zaehle. 2014. Implications of incorporating N cycling and N limitations on primary production in an individual-based dynamic vegetation model. *Biogeosciences* 11: 2027–2054. doi:10.5194/bg-11-2027-2014.

UCLouvain. 2017. Land Surface Seasonality. ESA Climate Change Initiative - Land Cover.

Vicente-Serrano, S. M., C. Gouveia, J. J. Camarero, S. Beguería, R. Trigo, J. I. López-Moreno, C. Azorín-Molina, E. Pasho, et al. 2013. Response of vegetation to drought time-scales across global land biomes. *Proceedings of the National Academy of Sciences* 110: 52. doi:10.1073/pnas.1207068110.

Wang, Y. L., X. Wang, Q. Y. Zheng, C. H. Li, and X. J. Guo. 2012. A Comparative Study on Hourly Real Evapotranspiration and Potential Evapotranspiration during Different Vegetation Growth Stages in the Zoige Wetland. *18th Biennial ISEM Conference on Ecological Modelling for Global Change and Coupled Human and Natural System* 13: 1585–1594. doi:10.1016/j.proenv.2012.01.150.

Waring, R. H., and S. W. Running. 2007. *Forest Ecosystems: Analysis at Multiple Scales.* 3rd ed. San Diego.

Weiss, J. L., C. L. Castro, and J. T. Overpeck. 2009. Distinguishing Pronounced Droughts in the Southwestern United States: Seasonality and Effects of Warmer Temperatures. *Journal of Climate* 22. Boston MA, USA: American Meteorological Society: 5918–5932. doi:10.1175/2009JCLI2905.1.

Wolf, S., W. Eugster, C. Ammann, M. Häni, S. Zielis, R. Hiller, J. Stieger, D. Imer, et al. 2013. Contrasting response of grassland versus forest carbon and water fluxes to spring drought in Switzerland. *Environmental Research Letters* 8. IOP Publishing: 035007. doi:10.1088/1748-9326/8/3/035007.

Wramneby, A., B. Smith, S. Zaehle, and M. Sykes. 2008. Parameter uncertainties in the modeling of vegetation dynamics—Effects on tree community structure and ecosystem functioning in European forest biomes. *Ecological Modelling* 216: 277–290. doi:10.1016/j.ecolmodel.2008.04.013.

Yoshimura, K., S.-T. Saiki, K. Yazaki, M. Ogasa, M. Shirai, T. Nakano, J. Yoshimura, and A. Ishida. 2016. The dynamics of carbon stored in xylem sapwood to drought-induced hydraulic stress in mature trees. *Scientific Reports* 6: 24513. doi:10.1038/srep24513.

Zhang, D., Q. Du, Z. Zhang, X. Jiao, X. Song, and J. Li. 2017. Vapour pressure deficit control in relation to water transport and water productivity in greenhouse tomato production during summer. *Scientific reports* 7: 43461. doi:10.1038/srep43461.

Zhang, K., J. S. Kimball, R. R. Nemani, S. W. Running, Y. Hong, J. J. Gourley, and Z. Yu. 2015. Vegetation Greening and Climate Change Promote Multidecadal Rises of Global Land Evapotranspiration. *Scientific Reports* 5: 15956. doi:10.1038/srep15956.

8 Appendix

Table S1: Western site daily growing season correlation analysis. Univariate and multiple linear regression of temperature (TMP), precipitation (PRE), and vapor pressure deficit (VPD). Spearman rho coefficient, R^2 adjusted R^2, and p-values. Asterisks indicate significant values.

Univariate	**Rho**	**R2**	**pVal**
TMP	0.002	0.001	0.9
VPD	-0.002	0.004	0.9
PRE	-0.0004	0.001	1
Multiple Linear Regression	**R2**	**Adj R2**	**pVal**
TMP Vs PRE	0.001	0.000	0.6
PRE Vs VPD	0.00	0.00	0.6
TMP Vs VPD	0.002	0.001	0.1

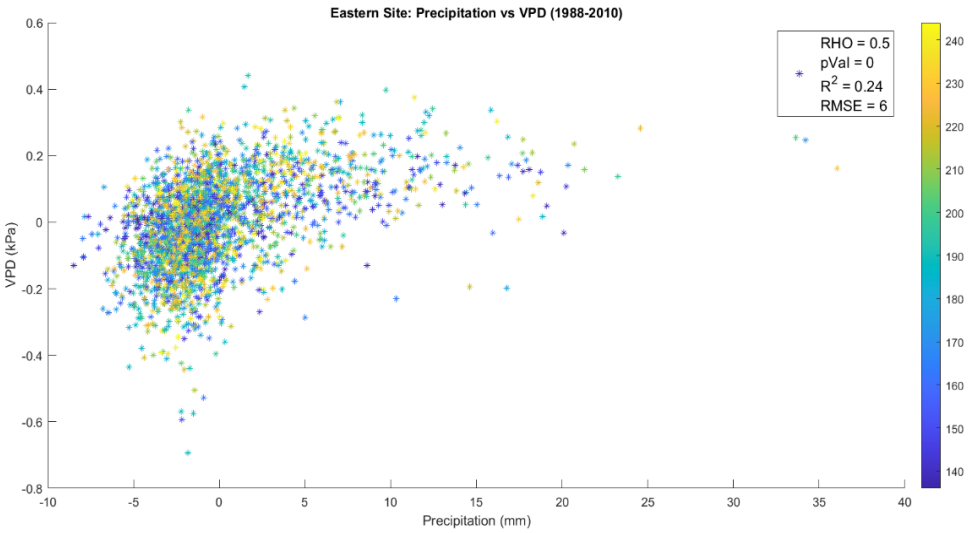

Figure S2: Eastern site, precipitation against vapor pressure deficit. Testing the influence of predictor variables against each other. Thus, the level of influence precipitation has on vapor pressure deficit levels at the eastern site.

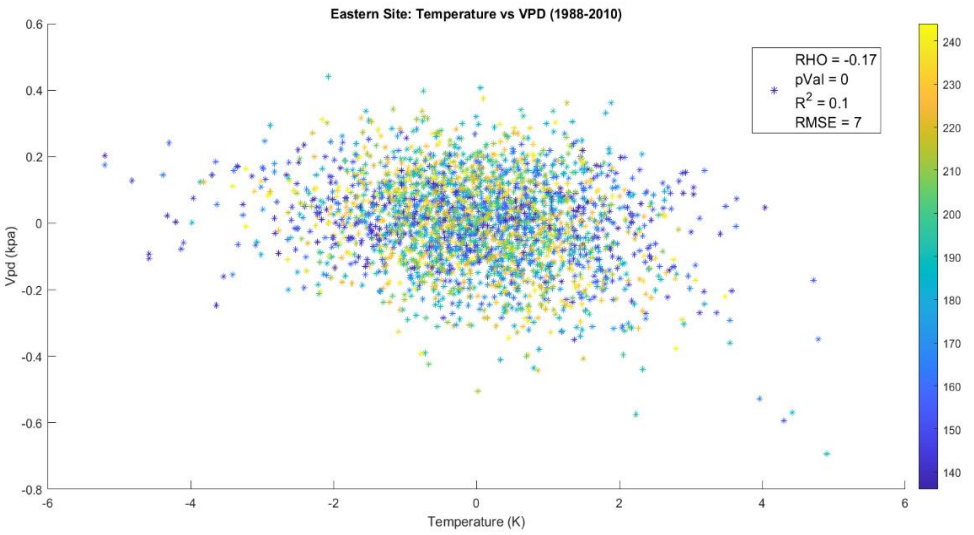

Figure S3: Eastern site, temperature against vapor pressure deficit. Testing the influence of predictor variables against each other. Thus, the level of influence temperature has on vapor pressure deficit levels at the eastern site.

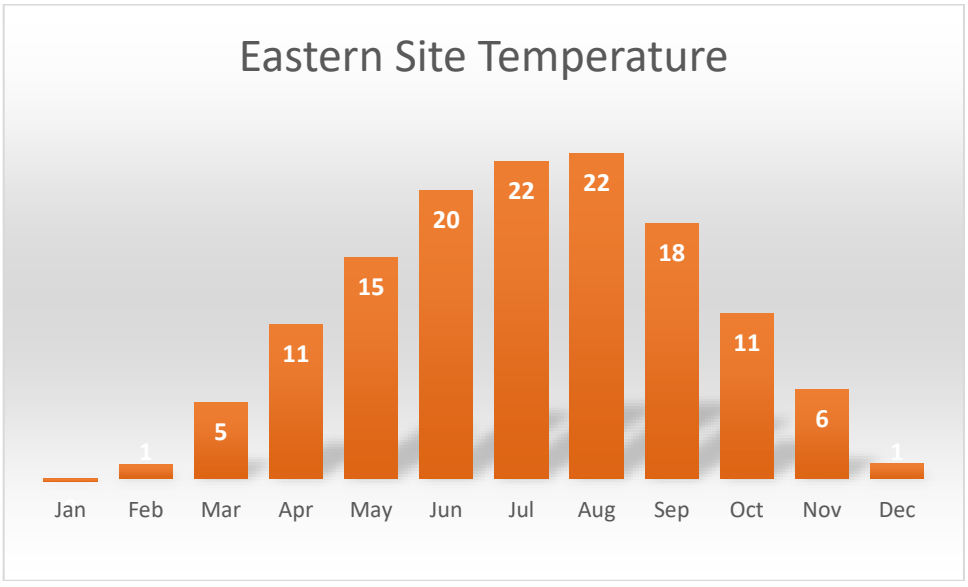

Figure S4: Eastern site, temperature variation across the months of the year (°C). Data retrieved from the Global Land Data Assimilation System (GLDAS, 2021).

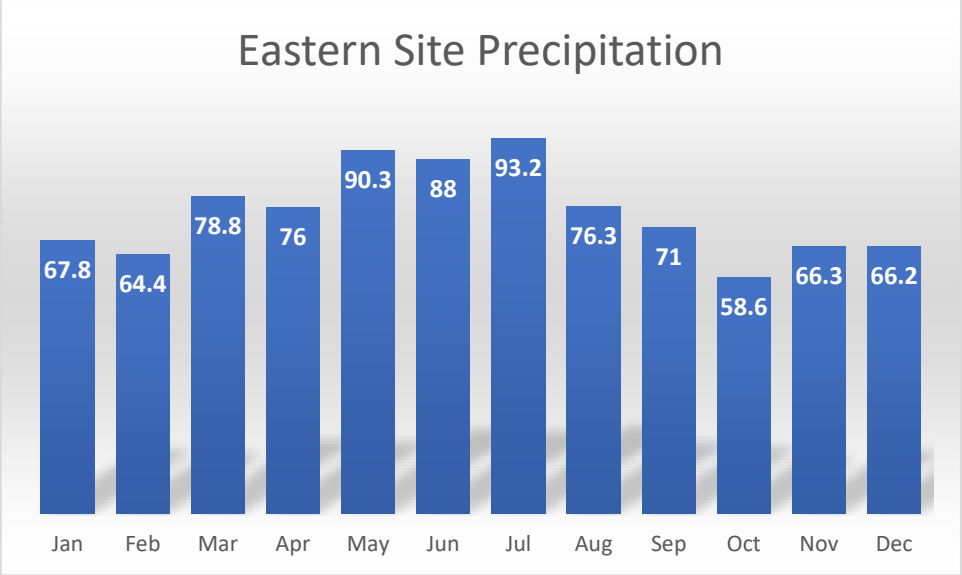

Figure S5: Eastern site, precipitation variation across the months of the year (in millimeters). Data retrieved from the Global Land Data Assimilation System (GLDAS, 2021).

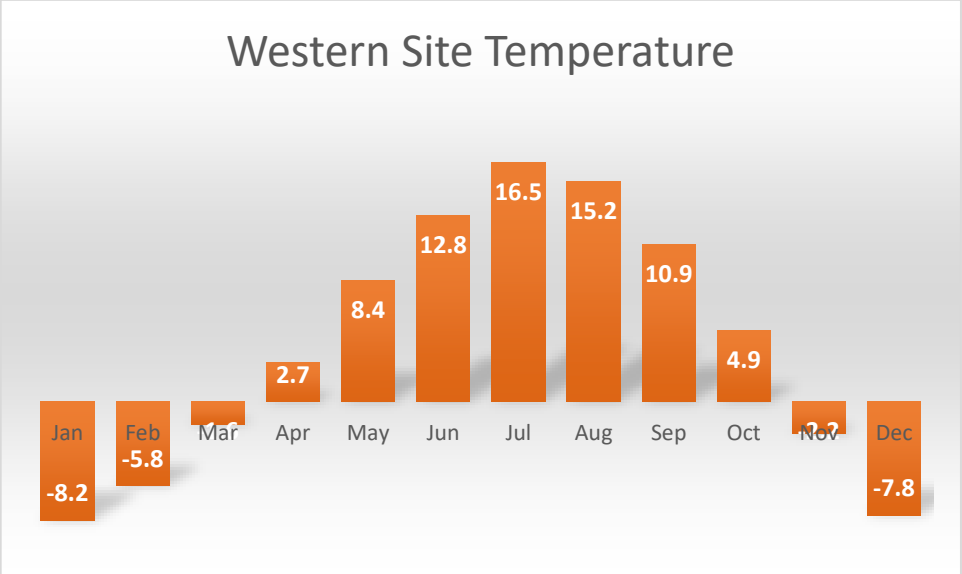

Figure S6: Western site, temperature variation across the months of the year (°C). Data retrieved from the Global Land Data Assimilation System (GLDAS, 2021).

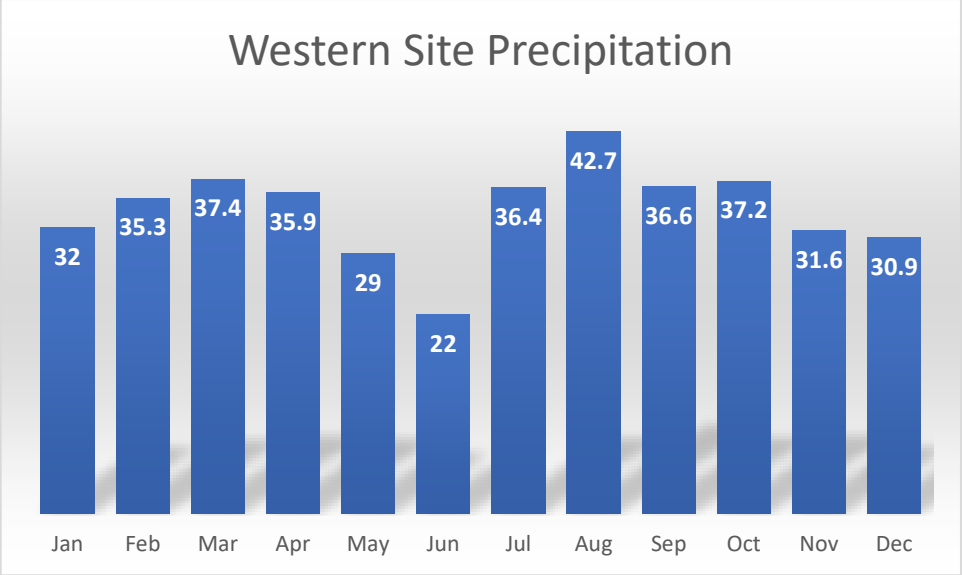

Figure S7: Western site, precipitation variation across the months of the year (in millimeters). Data retrieved from the Global Land Data Assimilation System (GLDAS, 2021).

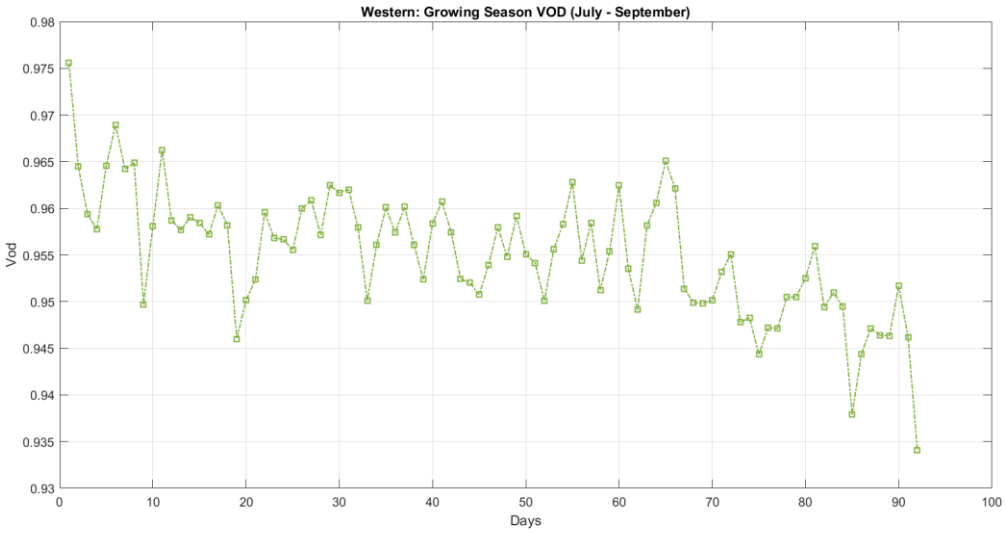

Figure S8: Western site, daily growing season VOD from July to September (1988-2010). This is to show evidence of declining VOD levels at the western site in September.